2026-04-22

Probing the Disequilibrium Chemistry of Two Late T-Dwarfs Using Planetary Intensity Code for Atmospheric Scattering

Crystal-Lynn Jacqueline Bartier
Brigham Young University

Probing the Disequilibrium Chemistry of Two Late T-Dwarfs Using Planetary Intensity Code for Atmospheric Scattering

Crystal-Lynn Jacqueline Bartier

A thesis submitted to the faculty of
Brigham Young University
in partial fulfillment of graduation requirements for the degree of

Master of Science

Denise Stephens, Chair
Benjamin Boizelle
Aleksandr Mosenkov

Department of Physics and Astronomy

Brigham Young University

ABSTRACT

Probing the Disequilibrium Chemistry of Two Late T-Dwarfs Using Planetary Intensity Code for Atmospheric Scattering

Crystal-Lynn Jacqueline Bartier
Department of Physics and Astronomy, BYU
Master of Science

We have performed a detailed analysis of the atmospheric properties of two late-T type brown dwarfs, 2MASSI J0415195-093506 and 2MASS J05591914-140448. For each brown dwarfs, we combined the spectra of each brown dwarf from the ground at 1-2.5 µm, AKARI at 2.5-5 µm, and from the Spitzer Space Telescope at 5-15 µm. For this project, we are particularly interested in probing the extent of vertical mixing. For this analysis, we used the Planetary Intensity Code for Atmospheric Scattering (PICASO), which is a code that creates a radiative transfer model for a given set of atmospheric parameters. With PICASO we find that metallicity has little effect on model fits, especially as it concerns modeling disequilibrium chemistry features. Vertical mixing and C/O, along with temperature, are parameters that play a significant role in creating accurate model fits to spectra. The best-fit PICASO models for the spectra of 2MASS 0415 and 2MASS 0559 struggle to accurately model the CO_2 absorption feature, which indicates that there is a need to improve understanding on what drives the observed CO_2 abundance.

Keywords: brown dwarfs, Spitzer, AKARI, atmospheric modeling, infrared spectroscopy, low-mass stars

ACKNOWLEDGMENTS

I would like to thank Dr. Denise Stephens, my mentor and advisor, for her support and guidance during this journey. Thank you to members of my committee, Dr. Boizelle and Dr. Mosenkov, for their feedback and support. Thank you to Dr. Lawler for allowing me to be one of her trusted minions. Also a big thank you to Savanah Turner and Zac Shakespear, whose support and help have been priceless. Thank you to my office mates for showing me how to make things look nice on LaTex. Thank you to BYU's Research and Writing Center, especially to Mary and Lisa, for helping me improve my writing and affirm my love of writing long sentences. Finally, I would like to extend my biggest gratitude to my family – my father, my brother, and my sister-in-law, and my close friends, for their unwavering love and encouragement.

Contents

List of Figures

List of Tables

Chapter 1

Introduction

This chapter will introduce brown dwarfs and their key spectroscopic characteristics. After introducing molecular lines and disequilibrium chemistry, I give a brief overview of this master's thesis.

1.1 History of Brown Dwarfs

Brown dwarfs were first conceptualized in 1963 by astrophysicist Shiv Kumar, who coined the term "black" dwarf to describe a substellar object that does not have enough mass to achieve the pressure and temperature to ignite nuclear fusion (Kumar 1963). Twelve years later, Jill Tarter changed the term from black dwarf to brown dwarf to avoid confusion with the successor of a white dwarf (Tarter 1985). Tarter described brown dwarfs as objects that are not massive enough to sustain hydrogen fusion, but are more massive or form differently from planets, with masses that do not exceed the hydrogen burning limit of about 0.08 $M_\odot$ (Kumar 1963).

In 1995, the first brown dwarfs were observed by two independent teams (Nakajima et al. 1995; Robello et al. 1995). Both teams conducted their research independently and on different brown dwarfs. Robello's team discovered their brown dwarf using the 0.80 meter diameter telescope at the

Teide Observatory in the Canary Islands by taking photometry of the Pleiades Star Cluster. They chose the Pleiades due to the young age of the population of stellar and substellar objects so that any brown dwarf observed would be younger and warmer, thus easier to observe. The brown dwarf that Robello's team discovered was aptly named Teide 1, a young M8-type object which would receive follow-up observation using spectroscopy to detect lithium in the atmosphere (Rebolo et al. 1996).

That same year, Nakajima's team observed an M-type star, GL229, and found that this red dwarf had a companion. Using spectroscopic observations in the optical and infrared wavelength ranges, Nakajima's team was able to confirm that GL229's companion, called GL229B, was a brown dwarf. The spectroscopic observations of GL229B revealed the prescence of water (H_2O) and methane (CH_4) in the infrared H (1.5-1.8μm) and K (2-2.4 μm) filters, which agreed with the theoretical models of brown dwarf atmospheres at that time.

Since 1995, brown dwarfs have been studied using both ground-based and space-based observations in the near-infrared. In 2003, the Spitzer Space Telescope (see Section 2.3) performed the first spectroscopic observations of brown dwarfs in the mid-infrared from 5-15 μm. Stephens et al. (2009) and Cushing et al. (2008), along with others, looked to quantify properties of the atmospheres of brown dwarfs such as temperature and cloud structure, but lacked spectral coverage in the 4-5 μm range to get a complete picture of brown dwarf atmospheres. With the AKARI Space Telescope (see Section 2.4), hereafter called AKARI, and James Webb Space Telescope (JWST), astronomers are able to fill in the 4-5 μm wavelength range to have a complete picture to study the atmospheric features of brown dwarfs.

1.2 Spectroscopy

Spectroscopy is the analysis of different wavelengths of light and allows for studies of atomic or molecular composition by the absorption or emission at specific wavelengths, as well exploration of an object's structure and other physical properties. Light, also called electromagnetic radiation, can be broken down into different types classified by energy and wavelength. Visible (optical) light ranges from 0.38 µm to 0.78 µm and is followed by infrared light, which ranges from 0.78 µm to 1000 µm. Brown dwarfs are best observed in the near and mid-infrared, from 1 to 15 µm because their cooler temperatures result in peak thermal emission at these wavelengths.

A spectrograph is an instrument that is attached to a telescope to break down light emitted from a source into the light's component colors, using a grism or a grating. From there, a camera records the spectrum of light, which contains information on the physics and chemistry of the source. The resolution of the observed spectra is determined by the diffraction grating, slit width, focal length, and the size of the pixels of the detector. The grating's groove density and size dictate the dispersion of light, while the slit width determines the amount of light entering and the maximum achievable resolution. In general, the longer the focal length and the smaller the detector pixels, the better the resolution.

As seen in Figure 1.1, the reduced spectrum of a brown dwarf consists of flux densities as a function of wavelength. Flux density is a measurement of the total energy from a source that is received onto a unit area over a wavelength interval over a time interval. The units of flux density and wavelength can vary. For this project we used units of Janskys (Jy) for flux and microns (µm) for wavelength.

All spectroscopic observations, regardless of if they are observed using ground or space-based telescopes, require careful inspection of the trace before the data is used for analysis (see Figure 1.2). The trace is the function that is used to define the central line of the target's light that is extracted and combined into a one-dimensional spectrum. When the trace is well-centered, it follows the target light on the detector and the extraction will include all the pixels illuminated by the target in the final spectrum. If the trace is not well-centered on the target spectrum, it can result in a large amount of background noise and can result in some (or all) of the target light getting cut off during the extraction, thus not measuring the total flux of the spectrum. An observation of a brown dwarf with a good trace means that the total flux of the object has been measured with minimal background noise contributing to the measurement.

For this project, the trace is important when looking to see which AKARI observations were good and which were not good (see Section 2.1), because the trace is not always well-centered fore each observation. AKARI uses an auto-generated reduction pipeline to define the trace, which is not verified by a human and is easily offset for low signal-to-noise data. Examples of a good and a bad trace from AKARI are presented in Figure 1.2 and in Figure 2.5, respectively.

1.3 Characterizing Brown Dwarfs

Brown dwarfs are defined as substellar objects that form via cloud collapse but unlike stars, brown dwarfs never become massive enough to sustain nuclear fusion in their cores. Instead they burn their limited supply of deuterium for a few hundred million years and then the fusion stops. Brown dwarfs differ from planets in that these substellar objects are thought to not share the same formation mechanisms as planets, which form through the core accretion process in the protostellar disk.

Brown dwarfs typically range from approximately 13 to 80 times the mass of Jupiter (Burrows et al. 2001), as that is the mass range at which deuterium fusion occurs. Brown dwarfs are classified into four spectral types in order of decreasing temperature: M (specifically, M.5 or later, with temperatures ranging from 2100–3500 K), L (1300–2100 K), T (600–1300), and Y (less than 600 K) (Marley & Robinson 2015). Spectral type classifications for brown dwarfs are based on the appearance of the spectra, which give information on molecular band strength and measured flux ratios. Molecular abundances in brown dwarf atmospheres change as temperature decreases. Spectral types of brown dwarfs are often denoted by a corresponding letter and a numerical value ranging from 0-10. Increasing number in a spectral class typically corresponds to decreasing temperature and luminosity. This study focuses on the physics and chemistry of T-types, and we discuss L-type brown dwarfs to help motivate this work.

L-type brown dwarfs, also referred to as L-dwarfs, are defined by the presence of metallic hydrides and neutral alkali metals in their optical spectra (Kirkpatrick et al. 1999) (see Figure 1.3). Infrared observations of L-dwarfs have shown that their atmospheres can contain carbon monoxide (CO) and water molecules (Cushing et al. 2006) along with silicate and iron (Fe) clouds (Burningham et al. 2021; Looper et al. 2008).

T-type brown dwarfs, also called T-dwarfs, are distinct from L-dwarfs due to CH_4 and H_2O molecules that dominate their atmospheres in the near-infrared from 1-2.5 μm (Burgasser et al. 2001) and (Burgasser et al. 2006b), as seen in the right panel of Figure 1.4. The increased strength of the Na I and K I doublet lines wipes out the flux in T-dwarfs in the optical, which prevents optical flux from being used to classify T-dwarfs. As such, T-dwarfs can only be classified with infrared spectra from 1-2.5 μm. Early T-dwarfs exhibit slowly dwindling CO bands and, as the T-dwarf spectral class progresses, H_2O and CH_4 bands strengthen in depth. The standard for late T-dwarfs is defined by the spectrum of 2MASSI J0415195-093506 (see the last spectrum on the right panel of Figure 1.4), where we see nearly saturated H_2O and CH_4 bands with sharp triangular flux peaks emerging between these bands. The progressive change in the spectral features of T-dwarfs is showcased in Figure 1.4.

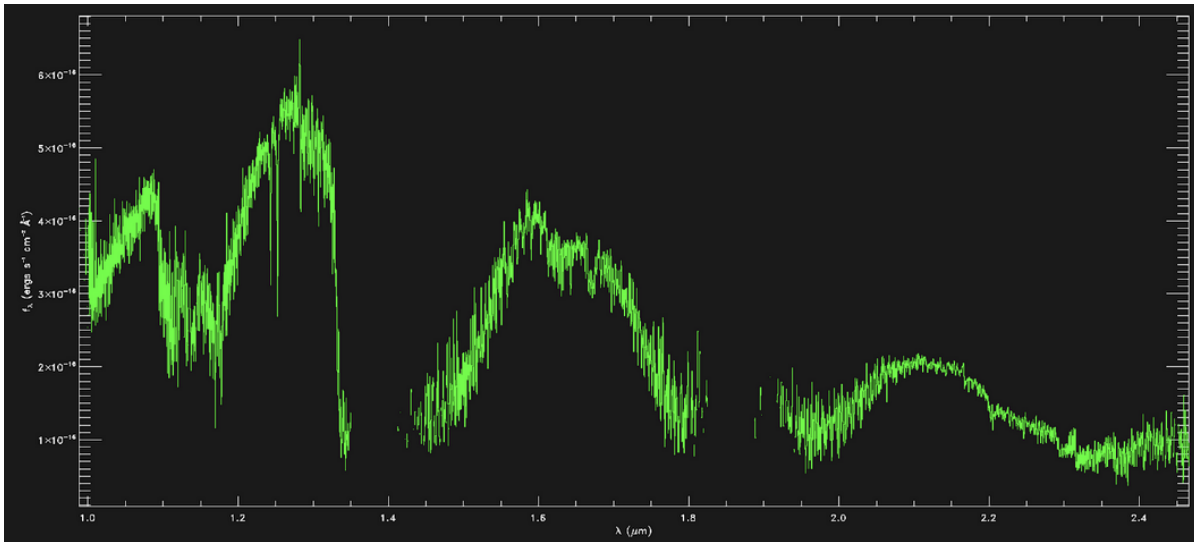

Figure 1.1 The reduced spectrum of a brown dwarf, SDSS 07584037+324724 from ground-based observations conducted at the Apache Point Observatory using the ARC 3.5 meter telescope with the TRIPLESPEC instrument. The gaps in the spectra are the result of removing regions that are significantly affected by telluric lines.

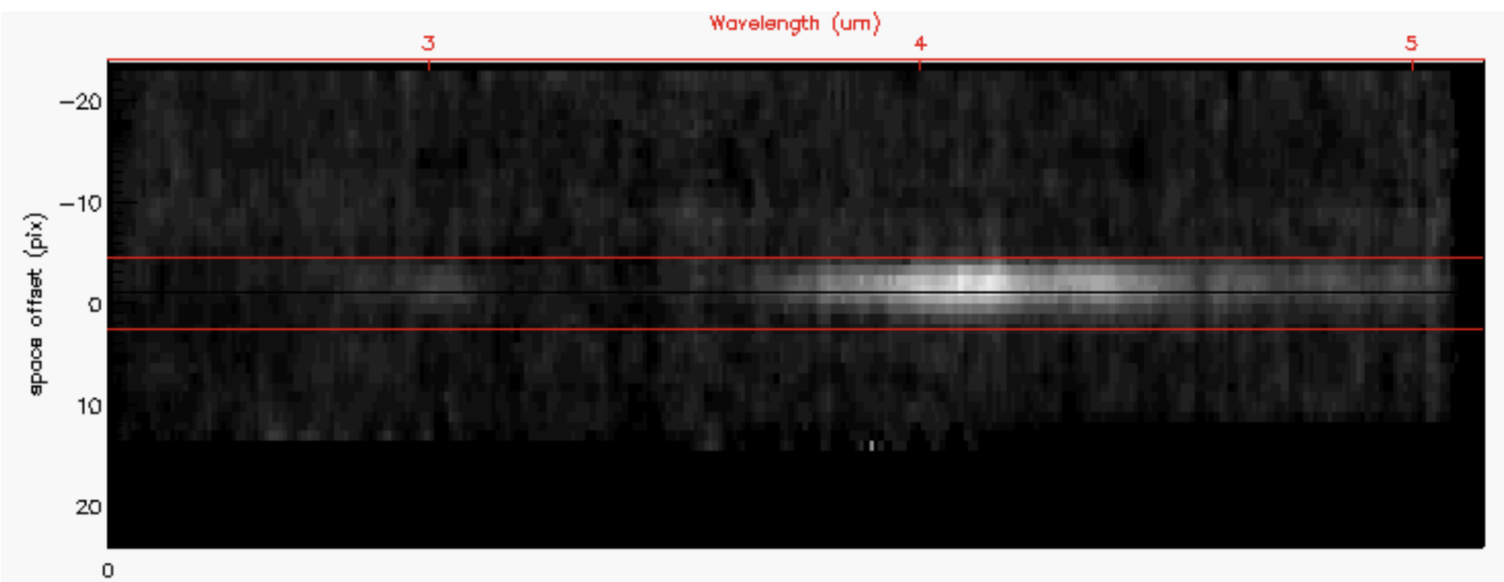

Figure 1.2 The trace and extraction window for one of the observations of 2MASSI J0415195-093506 using the AKARI Space Telescope. This is an example of a spectroscopic observation with a good trace because the trace captures all of the flux of the brown dwarf and there are minimal background pixels included in the extraction.

1.4 Disequilibrium Chemistry

In the early days of brown dwarf science, studies found that there are processes that occur faster than the timescale of key chemical reactions, which causes the composition of molecules in the atmosphere to be driven away from chemical equilibrium (Noll et al. 1997; Saumon et al. 2000). We call this disequilibrium chemistry, and it is caused by vertical mixing. Vertical mixing is the process in which molecules from lower (warmer) layers of the atmosphere are dredged up to higher (cooler) layers of the atmosphere. The pressure and temperature of a brown dwarf both increase with depth. Laboratory data shows that different molecules should be stable at different pressures and temperatures, so we would expect to see a variation in the dominant molecular species with atmospheric depth (Visscher & Moses 2011). For example, CH_4 is not expected to be present in the upper atmosphere of a hot L-dwarf because CH_4 bonds are too quickly broken in such a hot, energetic environment. CO, on the other hand, can more easily survive the hotter temperature of an L-dwarf upper atmosphere. In T-dwarfs with lower temperatures at higher levels of the atmosphere, molecules with weaker bonds can survive, such as those between carbon and hydrogen to make CH_4. When a T-dwarf is exhibiting vertical mixing, we see evidence of CO molecules being brought up from lower (warmer) layers of the atmosphere to higher (cooler) layers of the atmosphere (Lodders & Fegley 2002; Visscher & Moses 2011). We can see disequilibrium chemistry in T-dwarfs for the following pair of molecules: CO with CH_4, and ammonia (NH_3) with molecular nitrogen (N_2).

Equation 1.1 showcases how CO is converted into CH_4 in a brown dwarf's atmosphere, where CO and molecular hydrogen (H_2) create CH_4 and H_2O. At low temperatures ($\sim$800 K), we expect to see the abundance of CH_4 to dominate CO. When there is vertical mixing, CO is dredged up from lower (warmer) layers of the brown dwarf's atmosphere and does not break down quickly in the upper atmosphere as the C-O bonds take a long time to break down at lower temperatures. The CH_4 that is brought down to lower layers of the atmosphere is broken apart as the hydrogen bonds cannot survive the higher temperatures. This process is similar to what is seen with NH_3 and N_2, where vertical mixing causes N_2 to be dredged up from lower layers of the atmosphere and NH_3 is brought down to lower layers of the atmosphere. As such, we do not see as much NH_3 as we would expect. Equation 1.2 showcases the role that N_2 plays in the creation of NH_3.

$$CO + 3H_2 \rightleftharpoons CH_4 + H_2O \tag{1.1}$$

$$N_2 + 3H_2 \rightleftharpoons 2NH_3 \tag{1.2}$$

Vertical mixing drives species out of equilibrium, so any theoretical model that assumes chemical equilibrium will not be able to recreate the spectra we observe for these objects. The result of vertical mixing creates a spectral energy distribution that is difficult to study without creating a model that can account for disequilibrium chemistry. By using hybrid forward modeling (see Chapter 3), we can more accurately model the spectra of brown dwarfs to better understand the chemical processes that drive vertical mixing.

1.5 Project Overview

The goal of this project is to use state-of-the-art modeling methods to characterize the atmospheric features of two T-dwarfs from 1-15 μm. To do this, we employ PICASO (see Section 3.5) to explore in greater detail the extent of vertical mixing in these two T-dwarfs, so that we may further understand how certain model parameters, such as the ratio of carbon to oxygen and metallicity, affect the observed disequilibrium features. This project is uncommon as data from 2.5-15 μm range are rarely available. The work that is done here can not only be applied to brown dwarfs, but can also be used to characterize exoplanet atmospheres.

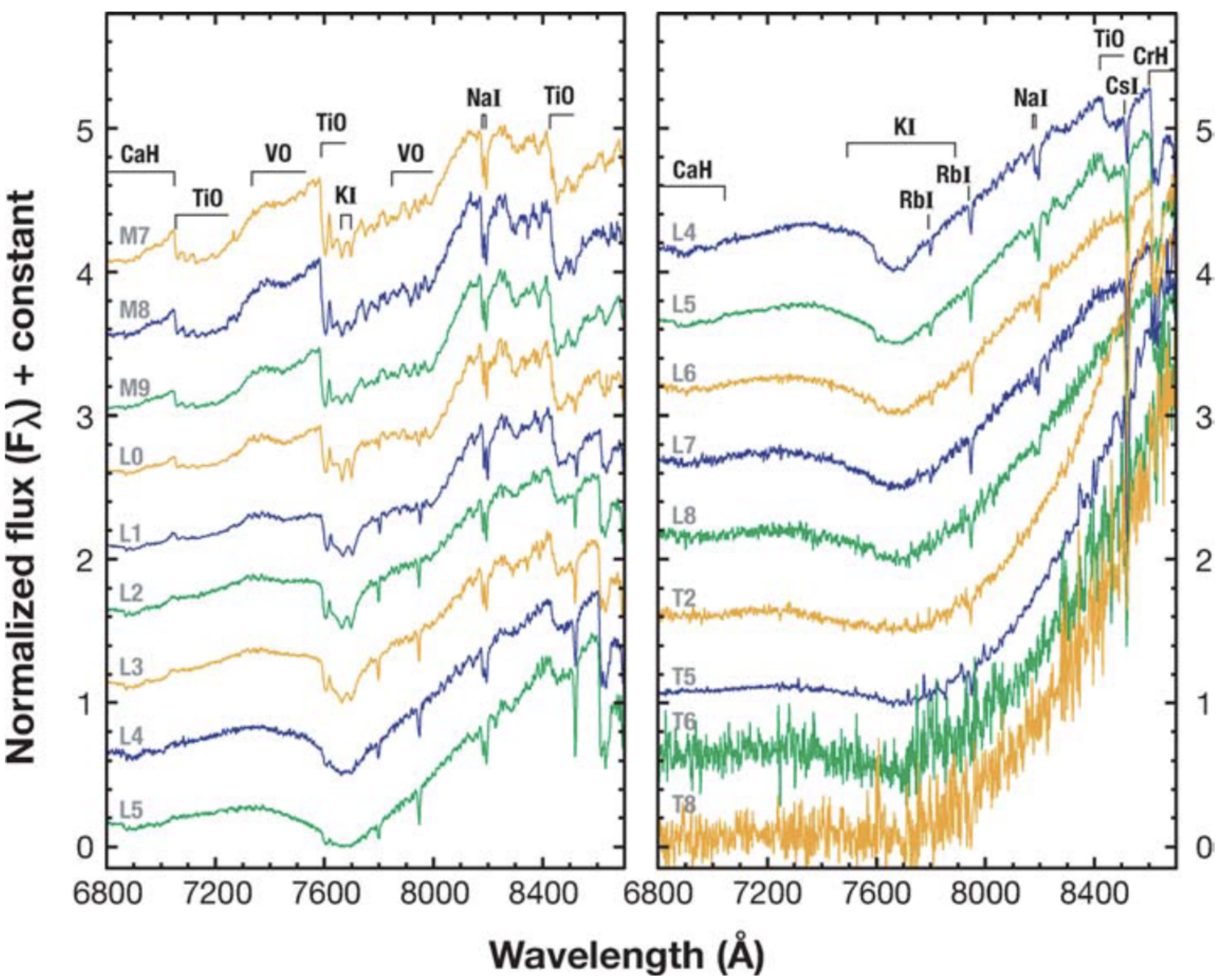

Figure 1.3 This figure is taken from Kirkpatrick (2005). The left panel showcases optical spectra of M-types transitioning to L-types with varying strength of the spectral features. The right panel showcases the optical spectra of brown dwarfs transitioning from L to T-types with varying strength of the spectral features. From the right panel, we can see that optical observations of later T-types are much nosier because these objects are intrinsically less luminous compared to M and L-types. Because T-types are so faint, they are best classified using near-infrared spectra.

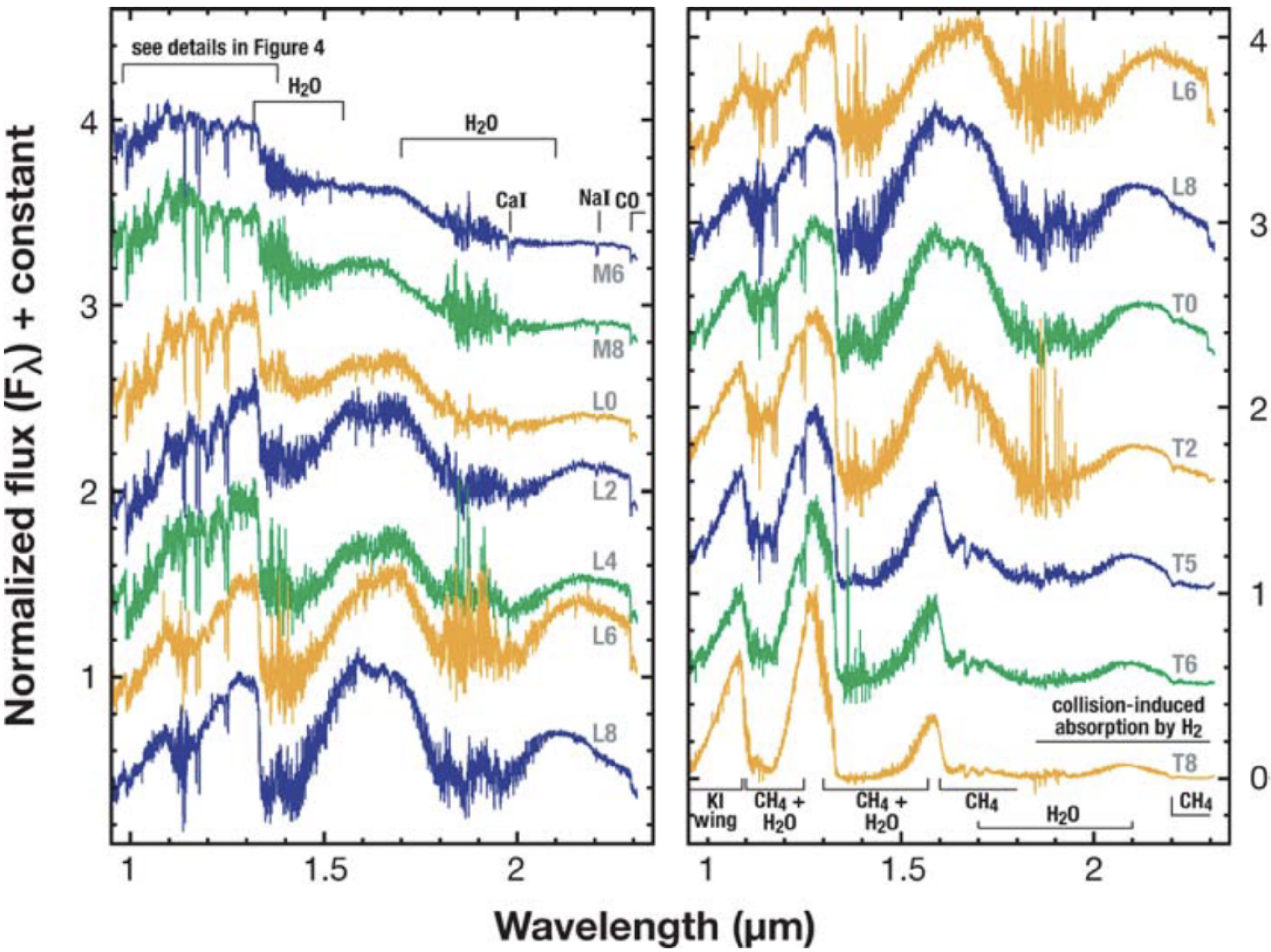

Figure 1.4 This figure is taken from Kirkpatrick (2005). The left panel showcases spectra of late M-type to L-types in the near-infrared and the growing depth of H_2O and CO bands. The right panel showcases the spectra of mid-L types transitioning to T-types and the appearance of CH_4. As brown dwarfs evolve, CH_4 begins to dominate over CO as the L-types transition to T-types. These spectra come from the Brown Dwarf Spectroscopic Survey archive by McLean et al. (2003).

Chapter 2

Data

In this chapter, we will briefly discuss the attributes of the two T-dwarfs in this study. Following the discussion on their fundamental properties, we will discuss the data that were used from telescopes to observe the spectra of these brown dwarfs. Additionally, this chapter discusses the history of the space telescopes from which spectroscopic data were used to analyze the disequilibrium chemistry of these two T-dwarfs. For this project, we used ground-based observations along with observations from two space telescopes, Spitzer and AKARI. In addition, we present the spectra for each brown dwarf of this study.

2.1 The Sample

As discussed in Section 1.5, the purpose of this study is to explore the disequilibrium chemistry of two T-dwarfs from 1-15 µm. This can be done by combining ground based, AKARI, and Spitzer observations. Many brown dwarfs have been observed from the ground, but fewer have been observed by spaced-based telescopes. As such, this study is limited to two T-dwarfs that have complete spectra from 1-15 µm. The result of these limitations and the science questions that we are looking to explore gives us our sample: 2MASSI J0415195-093506 (hereafter called 2MASS 0415) and 2MASS J05591914-140448 (hereafter called 2MASS 0559). 2MASS 0415 is a T8 brown dwarf while 2MASS 0559 is a T4.5 brown dwarf that is suspected to be a possible brown dwarf binary system (Cushing et al. 2008). 2MASS 0415 is located 5.7 pc (parsecs) from the Solar System, and 2MASS 0559 is 10.5 pc from the Solar System (Dupuy & Liu 2012).

2.2 Ground Based Observations

Brown dwarfs can be observed in the infrared using ground-based telescopes. Although ground-based telescopes have the potential to observe brown dwarfs from 1-5 μm, ground-based data from 2.5-5 μm is difficult to get due to Earth's atmospheric water lines (shown in Figure 2.1). As such, we are using ground-based data from 1-2.5 μm and using 2.5-5 μm AKARI observations, which is discussed later in this chapter.

The brown dwarfs in the sample of this project were both observed in the near-infrared (1-2.5 μm) using two different telescopes in the early 2000s. 2MASS 0415 was observed spectroscopically using the United Kingdom Infrared Telescope (UKIRT) on Mauna Kea (Knapp et al. 2004) and was the coolest brown dwarf to date at that time (see bottom panel of Figure 2.2). It was noted to have very deep near-infrared H_2O and CH_4 lines. 2MASS 0559 was observed spectroscopically using the NASA Infrared Telescope Facility (IRTF) SPeX instrument on Mauna Kea (Cushing et al. 2005). The CH_4 feature at 1.6 μm in the near-infrared spectrum of 2MASS 0559 (and 2MASS 0415) can be seen in the top panel of Figure 2.2.

2.3 The Spitzer Space Telescope

Spitzer was a space telescope launched in 2003 with the capability to observe celestial objects in the mid and far-infrared from 3-160 μm (Werner et al. 2004). Spectroscopically, Spitzer had the capability to observe from 5-40 μm. During the cold mission between 2003-2009, Spitzer observed brown dwarfs to help astronomers characterize mid-infrared spectra and bolometric luminosities. While ground-based near-infrared observations are limited in the near-infrared, due to the Earth's atmospheric absorption, Spitzer sets itself apart from ground-based observation in being able to observe the complex chemistry and cloud physics that occur in brown dwarf atmospheres without having to deal with Earth's atmospheric absorption.

In the earliest studies of brown dwarfs using Spitzer, Cushing et al. (2006) used the Infrared Spectrograph (IRS) to study features of M-, L-, and T- dwarfs (Y-dwarfs had not yet been discovered). They presented the first detection of NH_3 in the 10 μm band and the first detection of CH_4 in the 7.8 μm band. These observations would mark the early beginnings of studying the disequilibrium chemistry in mid-L-type dwarfs. In Figure 2.3, Cushing et al. (2006) presented 5-15 μm spectra of L-types transitioning to T-types and showcased the NH_3 disequilibrium feature around the 10 μm band.

Figure 2.4 showcases the 5-15 μm spectra of 2MASS 0415 (bottom panel) and 2MASS 0559 (top panel), respectively, that were observed using Spitzer. Both spectra for 2MASS 0415 and 2MASS 0559 contain the NH_3 absorption feature in the 10.3 μm band and the CH_4 absorption in the 7.8 μm band.

2.4 The AKARI Space Telescope

In 2006 a Japanese space telescope, AKARI, was launched with the primary objective to carry out an all-sky survey in the infrared (Murakami et al. 2007). The combination of all its instruments allowed AKARI to image and conduct observations from 2-180 μm. In this thesis, we use 2.5-5 μm observations from the Infrared Camera (IRC) (Onaka et al. 2007). AKARI's mission was retired in 2009 upon the completion of Phase 3, in which the cryocooler was allowed to continue only for near-infrared observations with the near-infrared camera (Sorahana & Yamamura 2012).

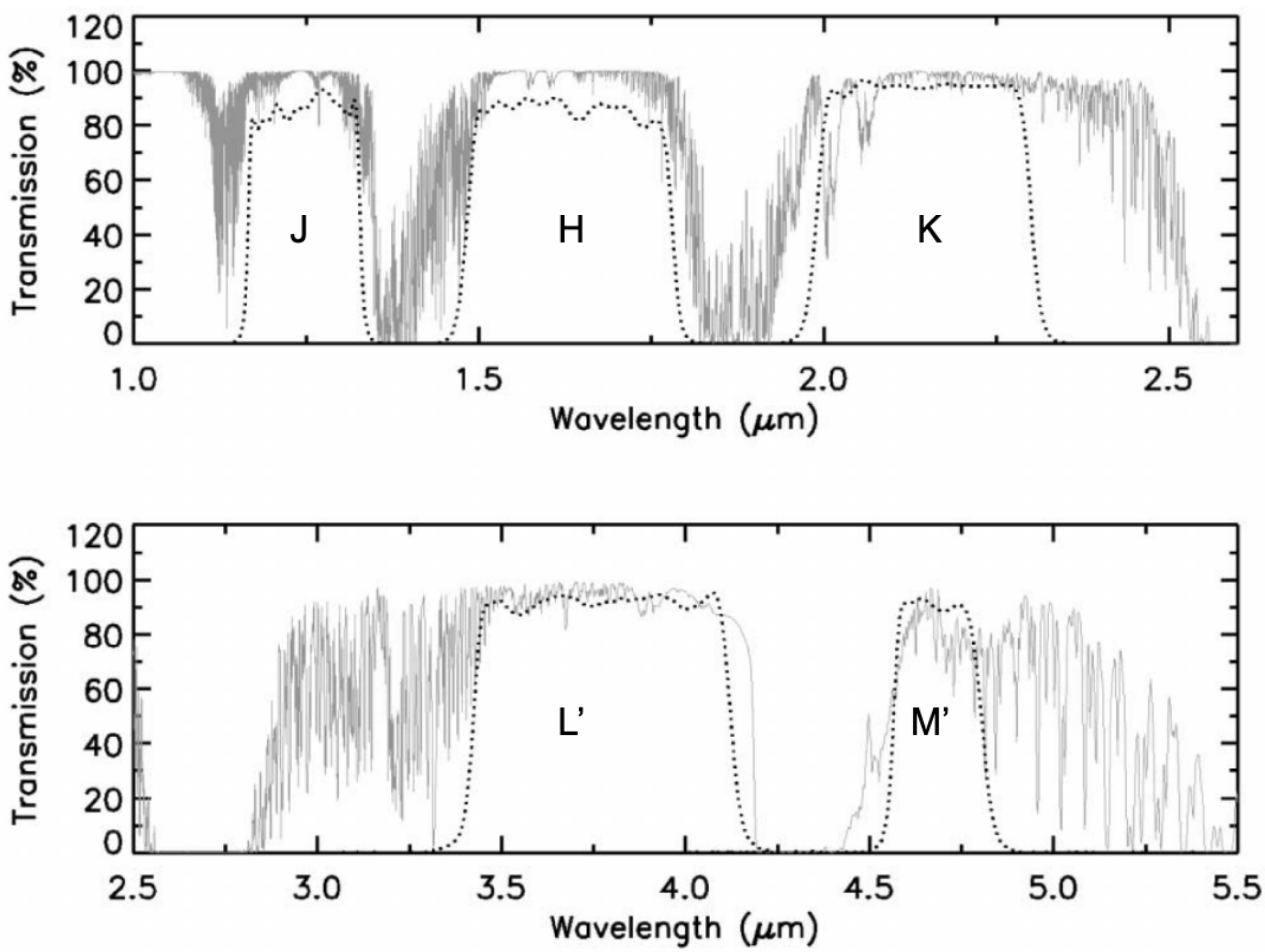

Figure 2.1 This figure is adapted from Tokunaga et al. (2002). The atmospheric transmission from the Earth at Mauna Kea is plotted as solid lines. The dotted lines are the spectral ranges for the filter profiles used at Mauna Kea Observatories. When the transmission drops to 0%, an object's flux cannot penetrate Earth's atmosphere. When the transmission is 100%, then an object's flux can pass through Earth's atmosphere. In the bottom panel, the 3-5 μm regime is dominated by transmission and emission from Earth's atmosphere, i.e. telluric lines. As such, important information is lost because of the absorption of Earth's atmosphere. Due to the strong presence of telluric lines from ground-based observations, there is a need for mid-infrared observations to be conducted using space-based telescopes in the 3-5 μm range.

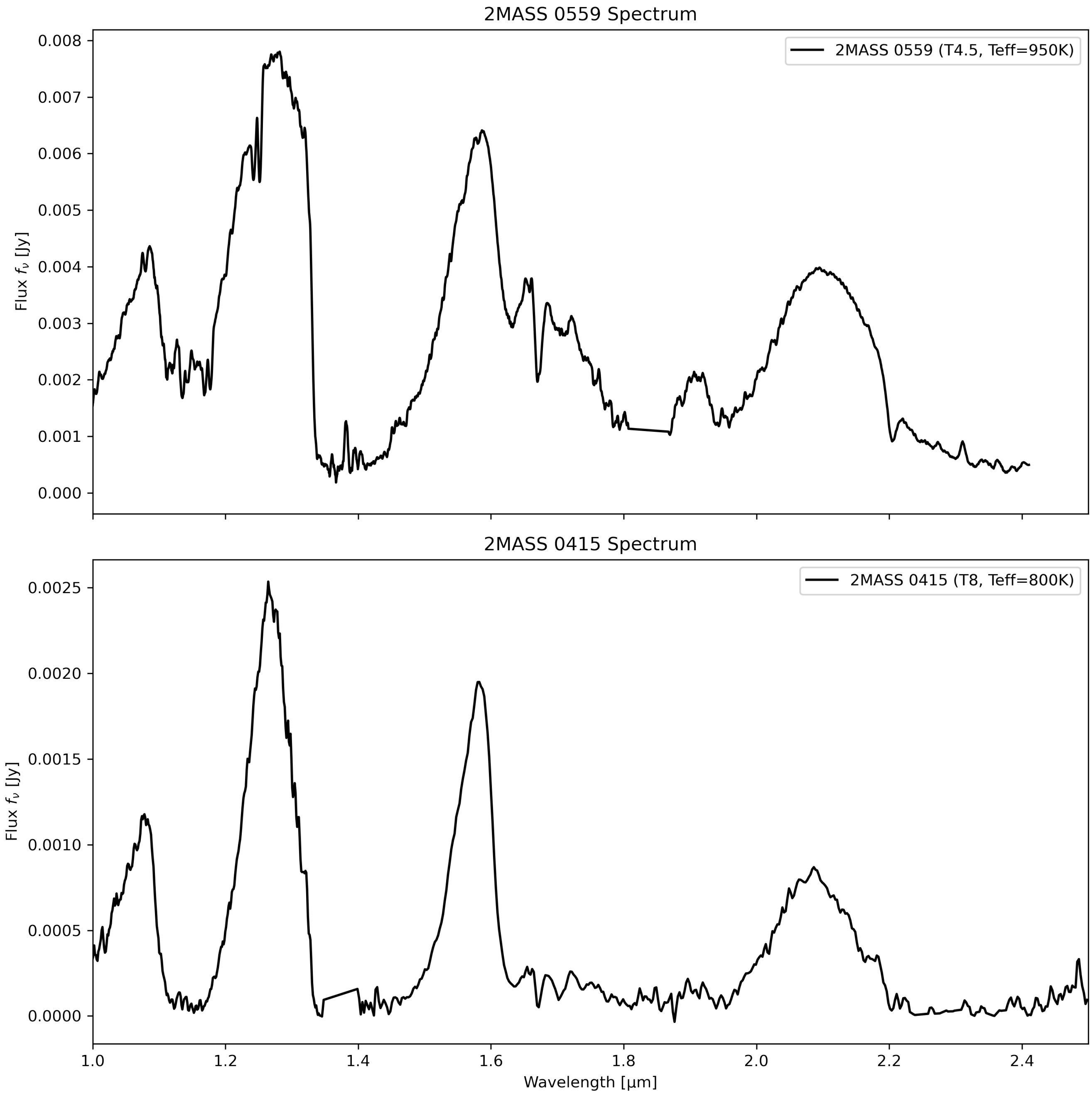

Figure 2.2 The 1-2.5 μm spectra of 2MASS 0559 (top) and 2MASS 0415 (bottom) from IRTF and UKIRT, respectively, plotted in black. This CH_4 absorption feature around 1.6 μm is so strong in the spectrum of 2MASS 0415 that it wipes out almost all of the photons from the brown dwarf at that wavelength.

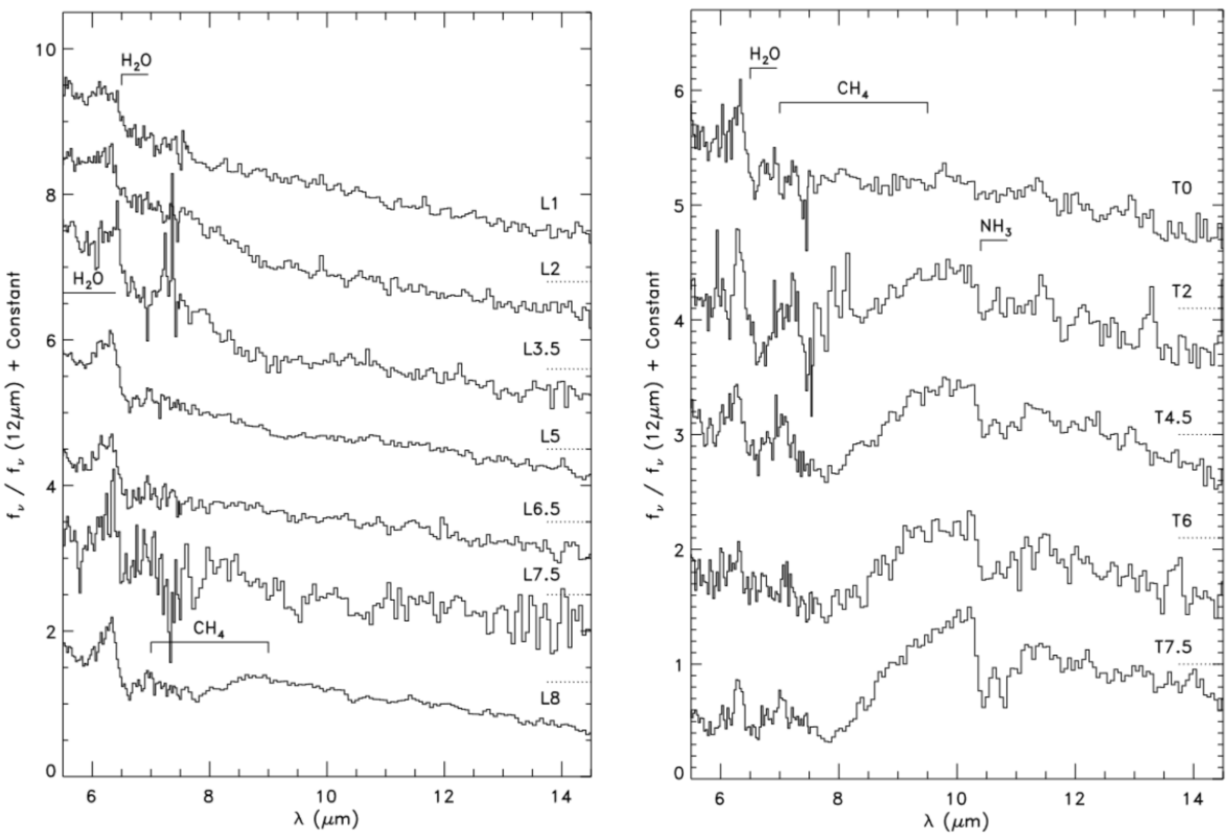

Figure 2.3 This figure was taken from Cushing et al. (2006). Spectra of L-type brown dwarfs with varying spectral types (left) and of T-types with varying spectral types (right) plotted in the mid-infrared. In these plots we can see the presence of CH_4 and NH_3 absorption at 7.8 μm and 10.3 μm, respectively.

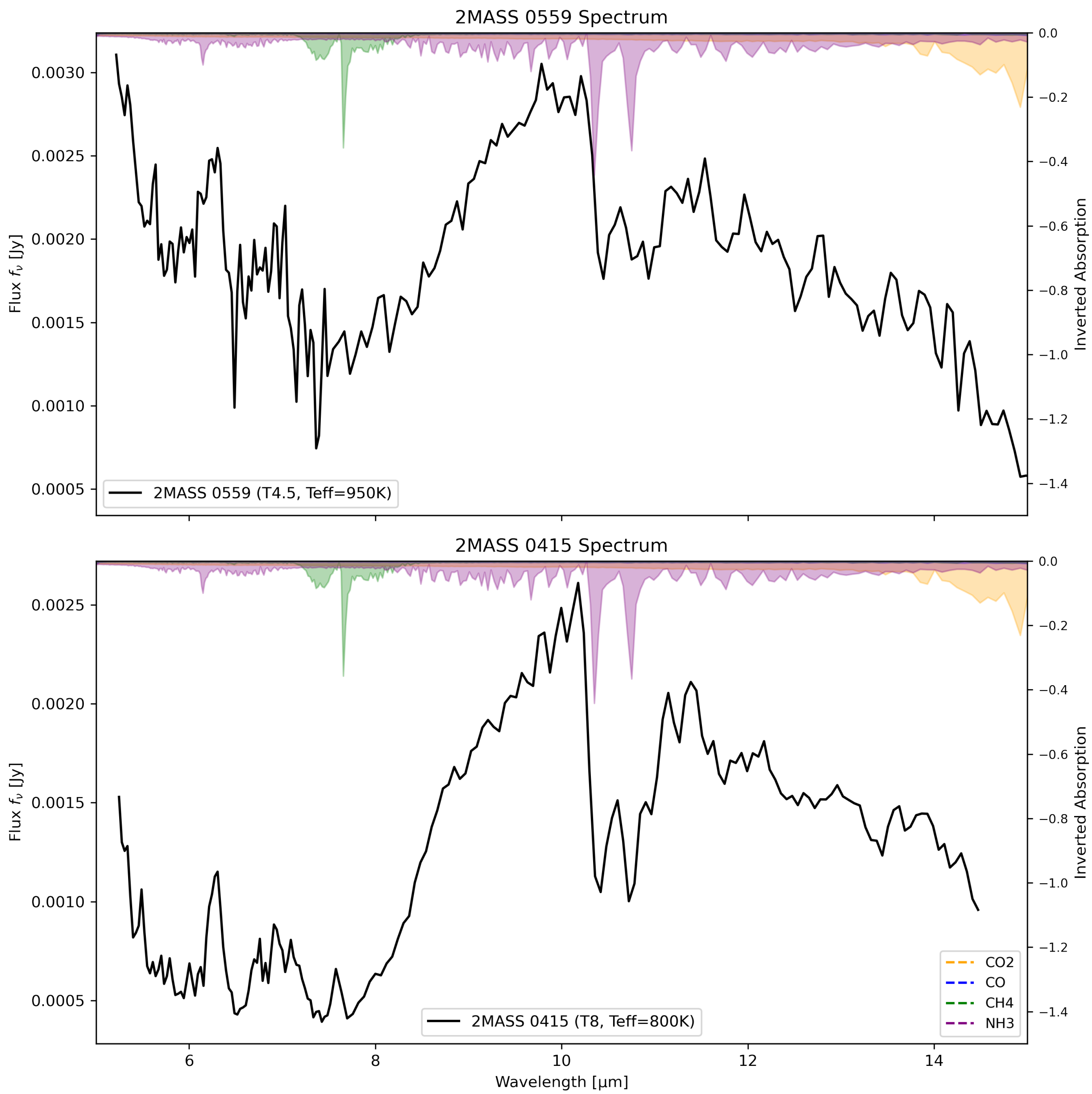

Figure 2.4 The 5-15 μm spectra of 2MASS 0559 (top) and 2MASS 0415 (bottom) plotted, along with the inverted absorption spectra of key molecules for this study: CH_4 (green), NH_3 (purple), and CO_2 (yellow). One of the two absorption features that are of interest to us, as it relates to disequilibrium chemistry, is the NH_3 absorption feature seen in the 10 μm band. In particular, we can see how the NH_3 absorption feature is much deeper for the cooler 2MASS 0415, compared to the warmer 2MASS 0559.

One of AKARI's key contributions was its spectroscopic observations of brown dwarfs from 2.5-5 µm. This is significant in that previously there was no spectroscopic space-based observations of brown dwarfs within this wavelength range and there would be no further observations in this band until the launch of JWST. AKARI observations highlighted the strengths of the molecular bands of CH_4 and CO_2 for L1 to T8-dwarfs within the 2.5-5 µm range (Sorahana & Yamamura 2012). Additionally, AKARI observations showed the first evidence of CO_2 in the spectra of late-L and T-dwarfs. Studying this spectral range in brown dwarfs allows for investigation of vertical mixing and carbon to oxygen ratio in brown dwarf atmospheres (Yamamura et al. 2010).

AKARI observed twenty-six brown dwarfs. Some of the brown dwarfs observed using AKARI had good signal to noise. In some of the archived AKARI data, we found that the trace on a number of observations was poor because of computer operation leading the trace to be misaligned. This led to poor-quality (or incorrect) spectra for some of these objects. When the trace is off (see Figure 2.5), the target's light is missed and additional background noise adds noise to the data, which cause artifacts, as seen in Figure 2.6.

Due to our interest in studying disequilibrium chemistry in brown dwarfs, the sample for this project is limited to T-dwarfs that have ground-based, Spitzer, and AKARI spectra, along with having a good trace and signal-to-noise. The 2.5-5 µm AKARI spectra of 2MASS 0415 and 2MASS 0559 can be seen in Figure 2.7.

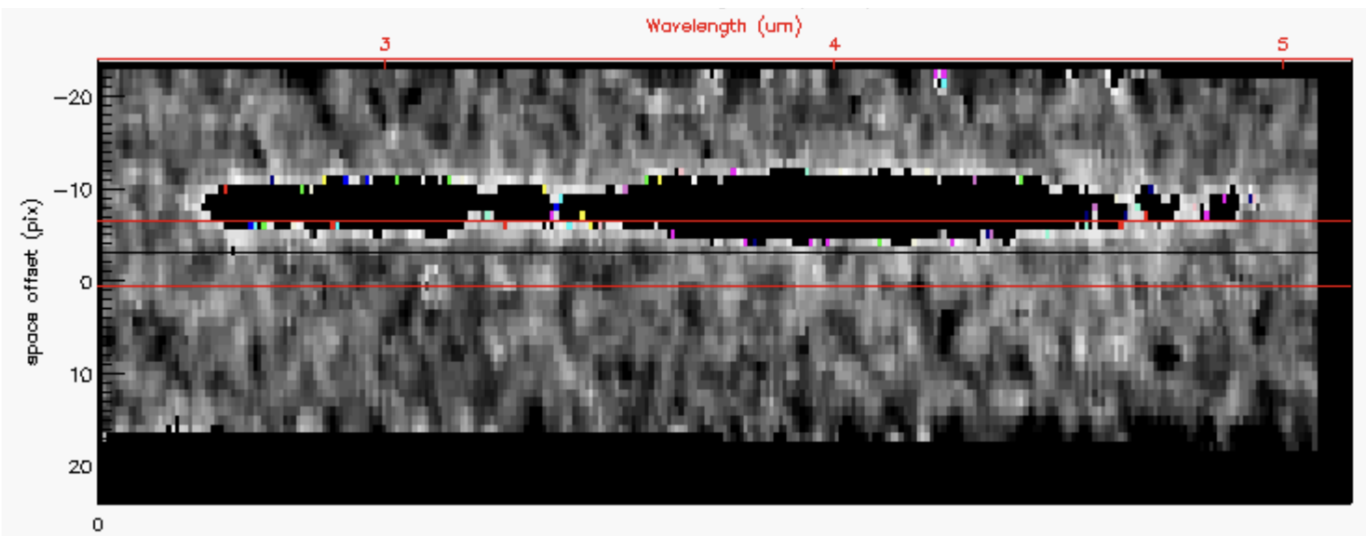

Figure 2.5 The trace for an observation and extraction window of SIMP J013656.5+093347 using the AKARI Space Telescope. This is an example of a spectroscopic observation with a misaligned trace calculated by the AKARI pipeline software, leading to missing target light and additional background noise in the final spectrum. Note, the object is so bright that the pixels are blacked out. The resulting spectrum for this observation can be seen in Figure 2.6.

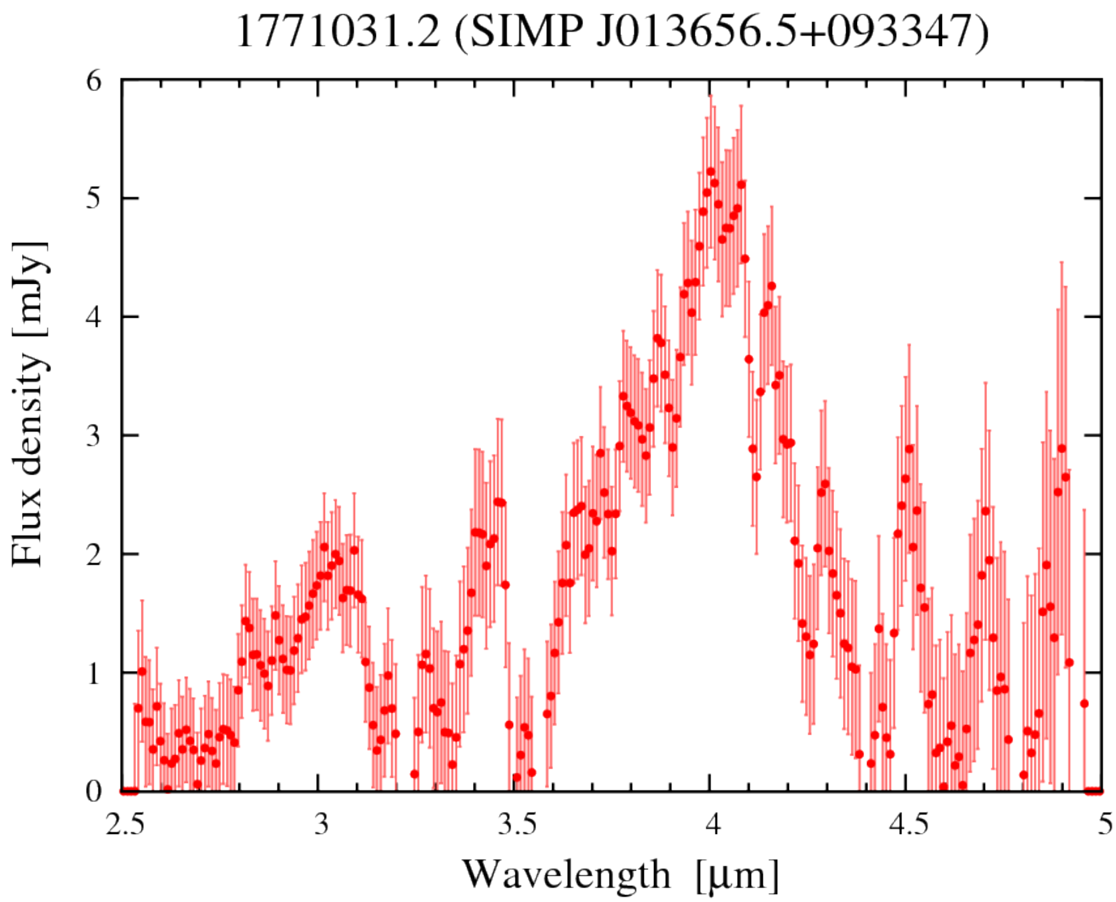

Figure 2.6 The AKARI spectrum of SIMP J013656.5+093347. The bars on the plot are indicative of upper and lower limits of the flux density measured using AKARI. Here we see the result of misalignment of the trace, which causes there to be poor signal-to-noise in the spectrum. The trace for this spectrum can be seen in Figure 2.5.

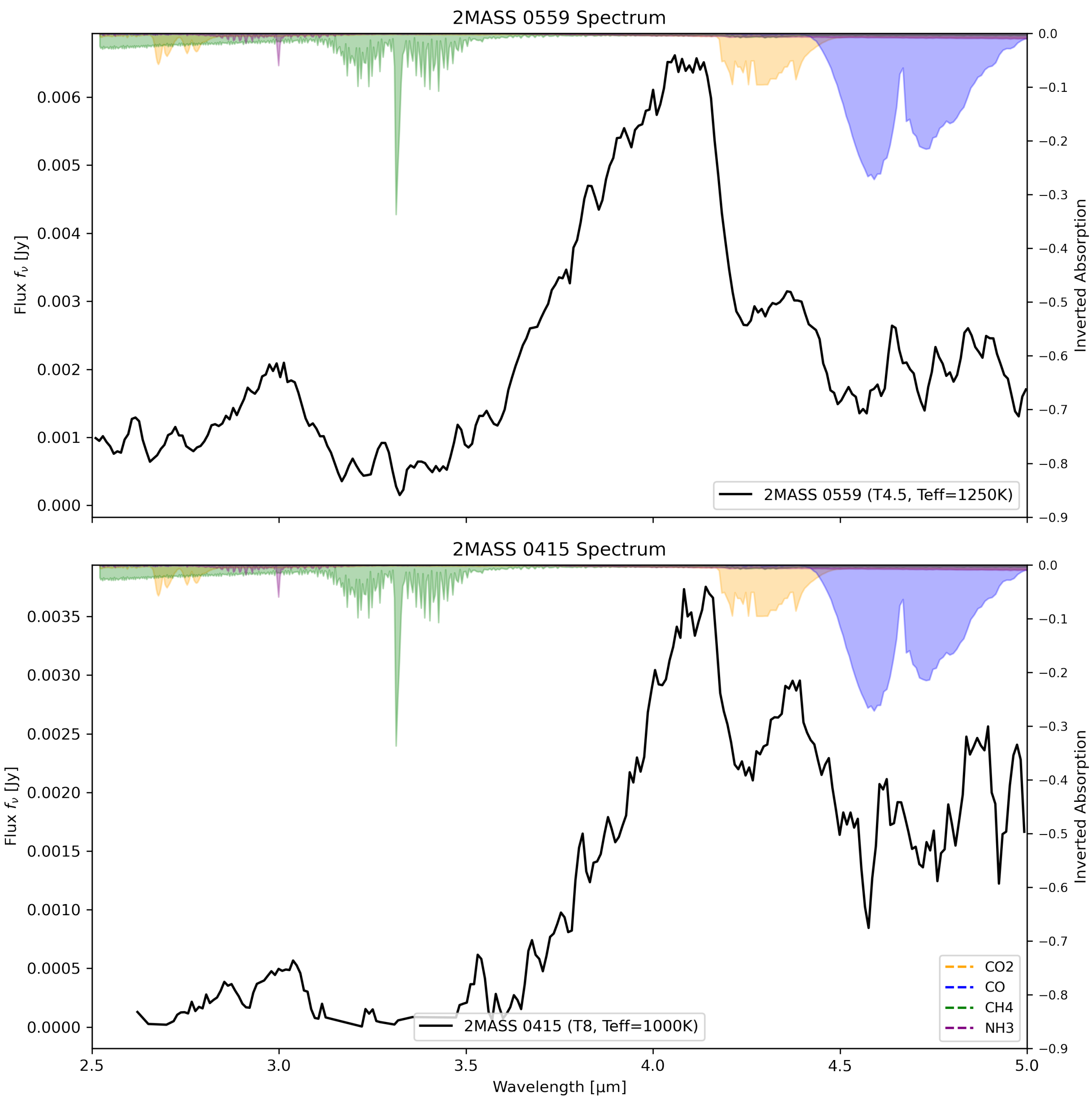

Figure 2.7 The 2.5-5 μm AKARI spectra of 2MASS 0559 (top) and 2MASS 0415 (bottom) plotted, along with the inverted absorption spectra of key molecules for this study: CH_4 (green), CO (blue), and CO_2 (yellow). The CO absorption feature in the 4.6 μm band and CO_2 absorption feature in the 4.2 μm band may help constrain the carbon to oxygen ratio.

Chapter 3

Theoretical Modeling

There are two approaches to modeling the atmospheres of brown dwarfs: forward modeling and retrieval modeling. This project employs forward modeling. In this chapter I discuss the model families, which include Sonora and Phoenix, their parameters, and how these modeling families compare to each other. Within those discussions, I explain the reason why certain model families were used for initial analysis. Later in the chapter, I introduce PICASO – a Python-based interactive hybrid of forward modeling that will serve as the primary use of forward modeling for this thesis.

3.1 Forward Modeling

One of the techniques used to calculate possible atmospheric properties of brown dwarfs is forward modeling. Using a self-consistent radiative transfer code, we generate models of atmospheres based on a simulation of a brown dwarf atmosphere structured in layers, with assumptions on the pressure, temperature, and molecular opacities at each layer (Marley & Robinson 2015). For each model that is calculated, we assume a metallicity, gravity, and carbon to oxygen ratio (C/O), which sets the chemistry of the atmosphere. For each atmospheric layer, we calculate the molecular abundance of molecules assuming chemical equilibrium. The model is constructed by atmospheric layer, where each layer is increasing in temperature and pressure with depth. For a given temperature and pressure, the code calculates which molecules should be present and an opacity coefficient which determines what percentage of photons will be absorbed at each wavelength. Given these assumptions, the radiative transfer code calculates how photons are absorbed, scattered, and emitted as they travel through the atmosphere to produce a final model spectrum.

Complexity can be added to a forward model by accounting for vertical mixing in the form of the eddy diffusion parameter. This parameter represents the speed and depth at which molecules are being dredged up from deeper layers of the atmosphere. Quenching occurs in upper layers of the atmosphere when the timescale of vertical mixing ($\tau_{\rm mix}$) is equal to or greater than the timescale of chemical reactions ($\tau_{\rm chem}$). This results in molecules that you would not expect being present in the upper atmosphere and the molecule that should be there being suppressed (i.e. quenched). When $\tau_{\rm chem}$ is less than $\tau_{\rm mix}$, then molecules in the upper atmosphere are in chemical equilibrium. When $\tau_{\rm chem}$ is greater than $\tau_{\rm mix}$, then the molecules are in chemical disequilibrium (Marley & Robinson 2015). For example, in the case of CO (see Equation 3.1), the effect of vertical mixing dredges up CO and causes there to be an overabundance of this molecule at higher layers of the atmosphere. We do not see an overabundance of CH_4 because the CH_4 is dragged to deeper (warmer) layers of the atmosphere and destroyed. The molecules driven out of equilibrium include CH_4 and CO, along with N_2 and NH_3 (see Equation 3.2). This type of forward model is in chemical disequilibrium. Figure 3.1 compares how forward models that are in chemical equilibrium and chemical disequilibrium differ by showcasing the depth of CO absorption for both aforementioned cases.

$$\mathrm{CO} + 3\mathrm{H_2} \rightleftharpoons \mathrm{CH_4} + \mathrm{H_2O} \tag{3.1}$$

$$\mathrm{N_2} + 3\mathrm{H_2} \rightleftharpoons 2\mathrm{NH_3} \tag{3.2}$$

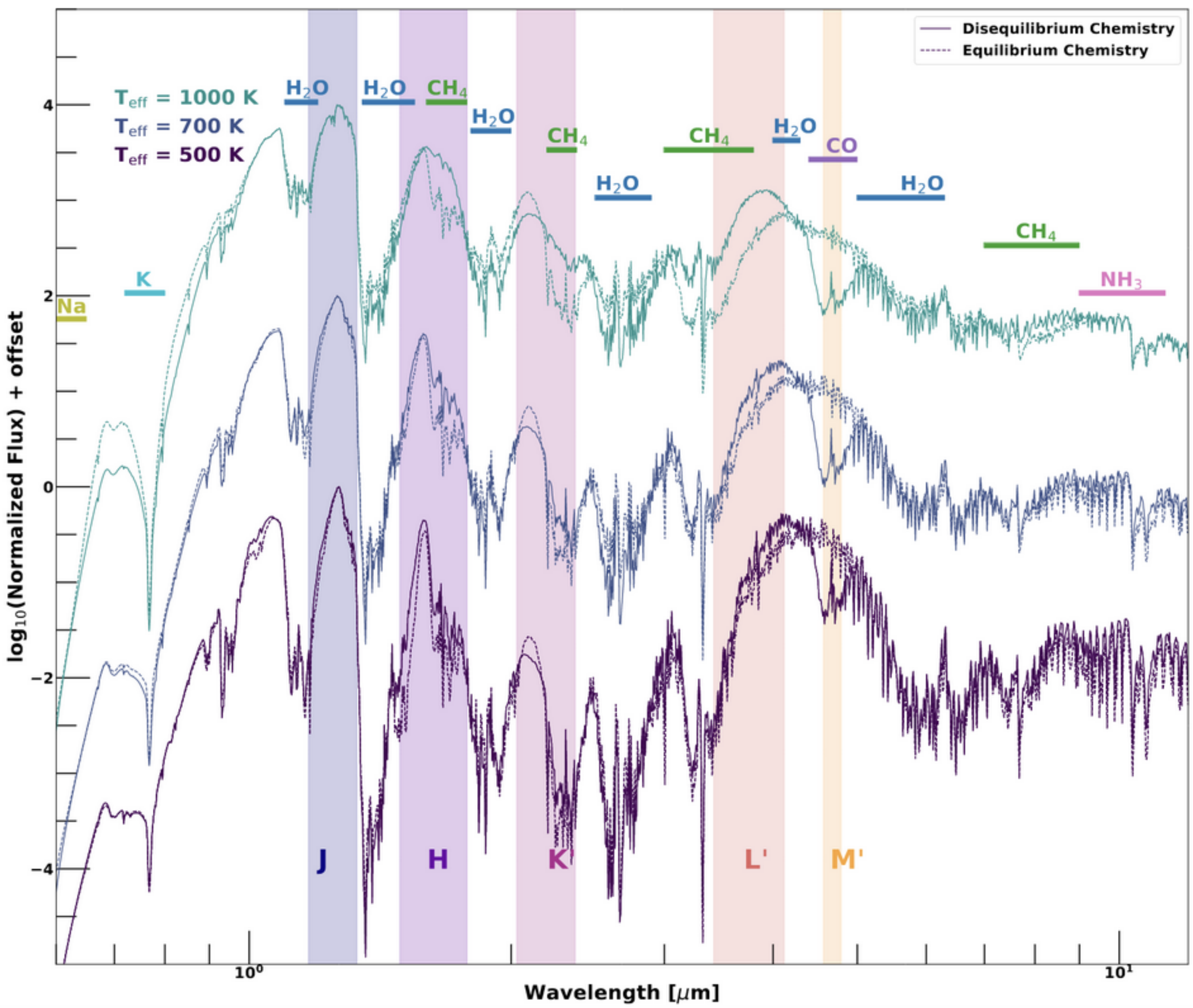

Figure 3.1 This plot was taken from Mukherjee et al. (2022). The model theoretical spectra of brown dwarf atmospheres change noticeably when applying either equilibrium (dashed line) or disequilibrium chemistry (solid line). Note the change in absorption strength for CO and CH_4 in the 3-5 μm region, which corresponds to the relative strength abundance of each molecule. With PICASO, the user can apply disequilibrium chemistry and freely vary other parameters, such as the presence of molecules in certain wavelength bands, to produce models that better-fit the observed spectra.

The advantage of forward modeling is that we can quickly compare grids of models to an observed spectrum using a chi-squared fitting algorithm. The disadvantage of forward modeling is that we are limited to the resolution of the parameters within the model grid. It is also not easy to interpolate between parameters and we are limited to the cloud models and molecules that were included in the forward models. For example, the Sonora and PHOENIX models have fixed ranges for parameters such as temperature, gravity and metallicity, and we cannot vary those values.

3.2 The Forward Models

To find the most probable values of temperature and gravity, we compared model spectra to observed brown dwarf spectra to estimate the most likely values for temperature and gravity. To do this, we take each theoretical model and compare each model one by one using a chi-squared algorithm (Cushing et al. 2008) to the observed spectrum. All models used for this project were regridded such that the spectral resolution of the models matched that of our data. The model spectrum is scaled to the observed spectra such that the deviation between the model and the data is minimized. This process is repeated for every single model. The model with the smallest deviation from the observed spectrum is the best-fit model.

The forward models used to make the best-fit have been pulled from various libraries: Sonora Bobcat (Marley et al. 2021), Sonora Cholla (Karalidi et al. 2021), Sonora Diamondback (Morley et al. 2024), Sonora Elf-Owl (Mukherjee et al. 2024), and Phoenix (Brock et al. 2021). The Sonora family and its code was built to model atmospheres for brown dwarfs and gas giant planets (Marley et al. 2021); (Karalidi et al. 2021); (Morley et al. 2024). The PHOENIX family (Brock et al. 2021) started as a grid of models used to study the atmospheres of stars along with novae and supernovae explosions, but now include brown dwarf atmospheres. In short, each group of models take a different approach to model the atmospheres of brown dwarfs. Additionally, each group of models has different ranges for temperature and do not cover the same parameter space. Table 3.1 gives a summary of ranges for effective temperature, clouds, [M/H], vertical mixing, and gravity for each group of models.

Table 3.1 This table showcases how the Sonora grid of model libraries compares to each other and to the PHOENIX grid of models.

Parameters of Forward Models					
	Effective Temperature (Kelvin)	Log(g) (cgs)	Clouds	Vertical Mixing (K_{zz})	Metallicity [M/H]
Sonora Bobcat	200-2400	2.5-5.5	None	None	-0.5 to 1.5
Sonora Cholla	500-1300	3.0-5.5	None	2, 4, and 7	-0.5 to 0.5
Sonora Diamondback	900-2400	3.5-5.5	1-8 (f_{sed})	None	-0.5 to 0.5
Sonora Elf-Owl	275-2400	3.25-5.5	None	2, 4, 7, 8, and 9	-1.0 to 1.0
PHOENIX	800-2000	3.5-5.5	1-10 (microns)	4 and 8	-0.5 to 0.5

3.3 Sonora Models

Table 3.1 outlines the parameters from the Sonora models. Before we go on to explain these models and how they fit in this thesis, we take a moment to explain some of the parameters. Surface gravity, hereafter called gravity, is in cgs units (i.e., centimeters, grams, and seconds) and is represented as log(g). For reference, Earth's log(g) is approximately 3 and the Sun's log(g) is approximately 4. Values for metallicity, hereafter denoted as [M/H], are generally in steps of 0.5 for the models in Table 3.1. A positive value of metallicity means that the brown dwarf has a higher percentage of metals than the Sun. A negative value of metallicity means that the brown dwarf has a lower abundance of metals compared to the Sun. The carbon to oxygen ratio (C/O) is also generally in steps of 0.5. Values of C/O that are greater than 1 are indicative of the atmosphere of a brown dwarf containing more carbon than oxygen, whereas values of C/O less than 1 tells us that there is more oxygen than carbon. For reference, the C/O of the Sun is 0.5.

The Bobcat models (Marley et al. 2021) are a grid of L-, T-, and Y-dwarf atmosphere models and are the first set of atmosphere models produced by the Sonora group. These were then followed by the Chollas (Karalidi et al. 2021), Diamondbacks (Morley et al. 2024), and Elf-Owls (Mukherjee et al. 2024). While the Bobcat models do not include vertical mixing, the Bobcats differ from previous models in that they include cooler temperatures and more diverse values for C/O abundances along with updated line opacities. Due to their lack vertical mixing, the Bobcats did not play a significant role in our analysis.

The Sonora Cholla models (Karalidi et al. 2021) are a grid of models that explore the disequilibrium chemistry in T-dwarfs (Burgasser et al. 2001) through the introduction of the eddy diffusion parameter, log(K_{zz}). A higher value of log(K_{zz}) is indicative of a brown dwarf atmosphere exhibiting more disequilibrium chemistry, whereas a lower value of log(K_{zz}) is indicative of less vertical mixing. These cloud-free models assume solar metallicity, [M/H]=0. The choice to not include clouds in the Cholla grid of models is because T-dwarfs are typically cloudless.

The Sonora Diamondback models (Morley et al. 2024) do not include a parameter to account for vertical mixing and instead focus on accounting for clouds in the form of the condensate sedimentation efficiency, which represents how "cloudy" a brown dwarf is. The condensate sedimentation efficiency is represented as f_{sed}. Lower f_{sed} values are indicative of a brown dwarf with thicker clouds with high opacity, while higher f_{sed} values are indicative of a brown dwarf with thinner clouds and lower opacity (Marley & Robinson 2015). As such, the Diamondback models are best suited to model warmer T-dwarfs and L-dwarfs that have more clouds (Knapp et al. 2004). While the Diamondback grid includes temperatures that could model 2MASS 0559, as seen in Chapter 4, we do not include them in our analysis due to the lack of accounting of vertical mixing.

The Sonora Elf-Owl grid is the newest grid of models from the Sonora family and was calculated using the PICASO radiative transfer code (see Sections 3.5 and 4.3) (Mukherjee et al. 2024). Due to time constraints, we do not use the Sonora Elf-Owl grid of models in our initial forward model analysis, but we do compare our results using PICASO to the Elf-Owls at the end of Sections 5.1 and 5.2. With values of K_{zz} that span across several orders of magnitude, various values for the C/O ratio, and sub-solar to super-solar metallicities, the Elf-Owl models look to explore the relationship between these three parameters as they model the disequilibrium chemistry of substellar atmospheres.

3.4 PHOENIX Models

The PHOENIX grid of models (Brock et al. 2021) that is used for this project began as a family of models that were created to explore the atmospheres of novae explosions (Hauschildt et al. 1992). In the following years, the original PHOENIX models evolved to study the atmospheres of more stable stars ranging from dwarfs to giants (Hauschildt et al. 1997); (Hauschildt et al. 1999). The iteration of the PHOENIX models used for this project include parameters that can simulate brown dwarf atmospheres and contain the following parameters: effective temperature, gravity, vertical mixing, clouds, and metallicity. Instead of f_{sed}, the PHOENIX models calculate a brown dwarf's "cloudiness" via the measurement of the radius of cloud particles. As seen in Table 3.1, these values range from 1 to 10 microns.

3.5 PICASO

To create our own radiative transfer models, we implement the Planetary Intensity Code for Atmospheric Scattering (PICASO). PICASO is a Python-based interactive hybrid used to create forward models that allows its user to input physical parameters to create a new atmospheric model (Mukherjee et al. 2023). To use PICASO, the user inputs physical parameters, such as temperature and gravity, to create a new radiative transfer model with those values. The code assumes radiative-convective equilibrium and produces a spectrum corresponding to the the input parameters. Additionally, PICASO allows its user to add in molecular features and clouds to create forward models. In short, with PICASO a user can create their own library of models. Figure 3.1 showcases an example of the differing models for various temperatures using PICASO and illustrates how models of substellar atmospheres change when modeling disequilibrium versus equilibrium chemistry.

PICASO is a code that is updating and evolving as our understanding of planetary and substellar atmospheres improves. We have chosen PICASO to model the atmospheres of 2MASS 0415 and 2MASS 0559 as PICASO allows its users to create their own library of models using the current understanding of the physics and chemistry of brown dwarfs. Specifically, PICASO allows us to hold some parameters fixed, while varying other parameters to better understand the relationship between log(K_{zz}) with C/O, [M/H], and temperature.

Additionally, PICASO allows us to better constrain how certain parameters, such as vertical mixing and the C/O abundances, are modeling key absorption features. For example, if C/O is greater than 1 (i.e., more carbon), then we may see more CH_4 in the atmosphere. If C/O is less than 1 (i.e., more oxygen), then we may see more CO_2. C/O may be different depending on how the brown dwarf formed (Beiler et al. 2024b). We allow the C/O abundances to vary relative to the Sun because brown dwarfs potentially have different formation mechanisms, such as disk accretion (like planets), or cloud fragmentation (like stars).

The version of PICASO that is used for this project is version 3.2, which was the version of PICASO that was used to create the Sonora Elf-Owl grid (Mukherjee et al. 2024). The starting PICASO parameters for 2MASS 0415 and 2MASS 0559 come from the best-fit forward modeling results, which are discussed in further detail in Chapter 4.

Chapter 4

Methodology

In this chapter, I discuss the steps taken to analyze the atmospheres of 2MASS 0415 and 2MASS 0559 using PICASO. Once the data is prepared for analysis, I discuss the process of using the best-fit Sonora forward models to produce initial parameters to input into PICASO to create more complex model fits for each brown dwarf spectrum. Lastly, this chapter details how PICASO was used to create disequilibrium fits for 2MASS 0415 and 2MASS 0559.

4.1 Data Preparation

Both 2MASS 0415 and 2MASS 0559 had two observations each from AKARI. The observations with the best signal to noise (S/N) spectrum were chosen for analysis. The associated AKARI observations of 2MASS 0415 and 2MASS 0559 that were used for this project are plotted in Figure 2.7. After selecting one observation for 2MASS 0415 and 2MASS 0559, the data were prepared for analysis. The ground-based and Spitzer observations of 2MASS 0415 and 2MASS 0559 were studied previously (Cushing et al. 2006; Knapp et al. 2004; Stephens et al. 2009) and the processed data was obtained from these groups.

Upon choosing the AKARI observations with the best S/N spectrum and converting their flux values, we ensured that the observations with good trace were flux-calibrated correctly by comparing known flux-calibrated ground-based data from 3-4 μm (Cushing et al. 2006), with the AKARI observations for 2MASS 0415 and 2MASS 0559. Figure 4.2 showcases the visual confirmation that the AKARI spectrum for 2MASS 0415 was accurately flux-calibrated. Since the known flux -alibrated ground-based data aligned with AKARI observations of 2MASS 0415 and 2MASS 0559, additional flux calibration was not needed for the AKARI data.

The last step in preparing the data for analysis involved stitching together the ground and space-based spectra using the 1-2.5 μm, 2.5-5 μm, and 5-15 μm spectra to create two text files with the combined spectrum for 2MASS 0415 and 2MASS 0559. In removing the negative flux from the AKARI observations of 2MASS 0415, there is a small gap between where the ground-based observations ended at 2.5 μm and where the usable AKARI observations began at 2.6 μm. For 2MASS 0415, there is another gap in the transition from AKARI to Spitzer data between 4.99 μm and 5.2 μm. For 2MASS 0559, there is no gap between the ground-based and AKARI observations but there is a small gap between 4.99 μm and 5.18 μm. For visual purposes, these gaps are always plotted with an artificial line that has no impact on modeling the spectra of these T-dwarfs. The resulting combined spectra of 2MASS 0415 and 2MASS 0559 are plotted in Figure 4.3.

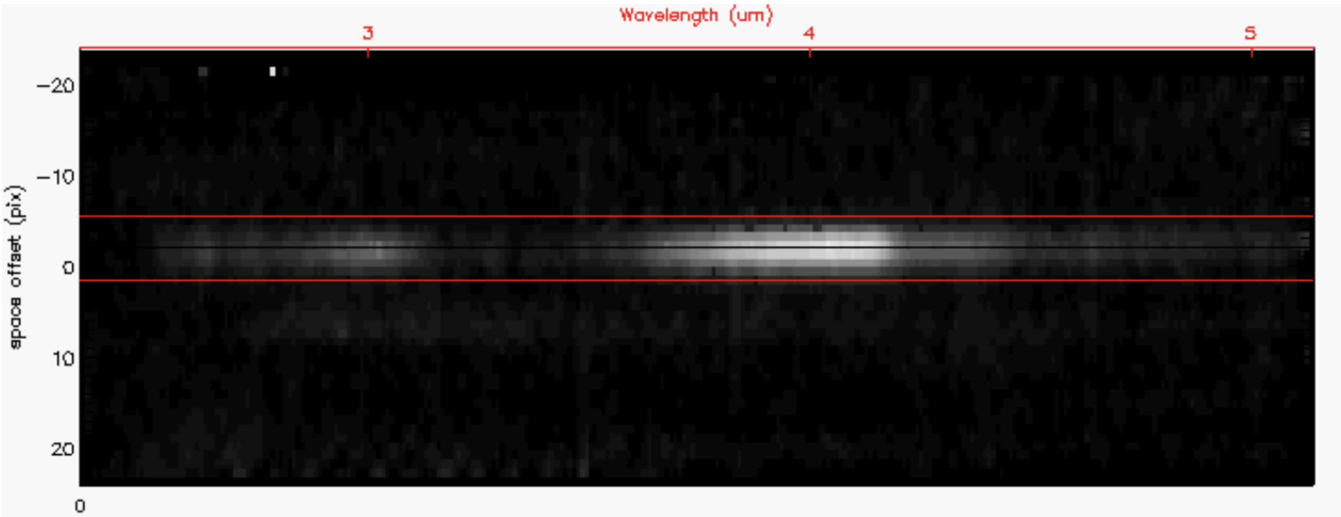

Figure 4.1 A good trace for one of the observations of 2MASS 0559 using the AKARI space telescope (black line) and extraction window (red). The corresponding spectra to this trace is included in Figure 4.3.

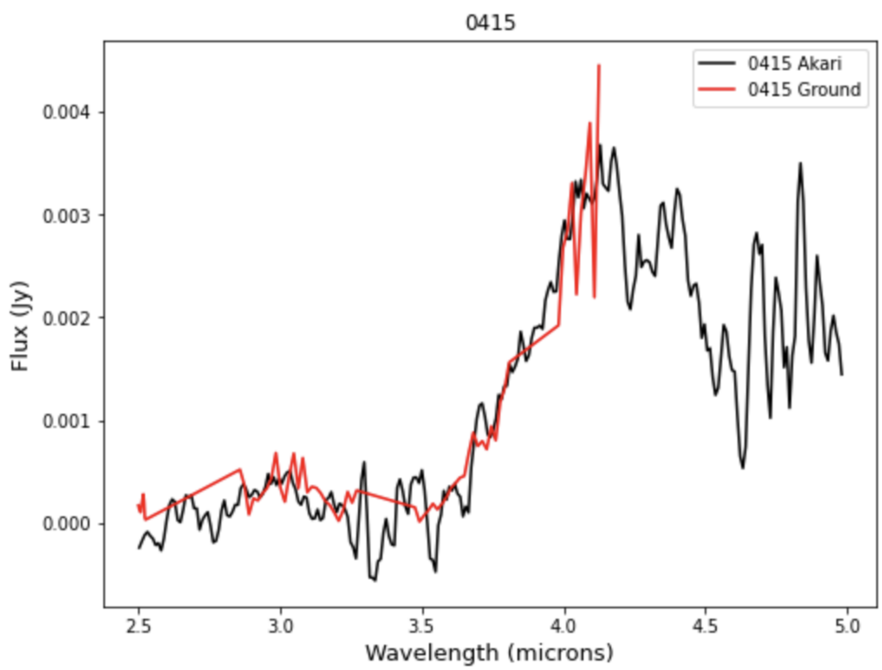

Figure 4.2 The 2.5-4 μm ground spectrum from Cushing et al. (2006) (red) plotted with the 2.5-5 μm AKARI spectrum (black) of 2MASS 0415. The overlay of these two spectra showcase that the AKARI data was accurately flux calibrated.

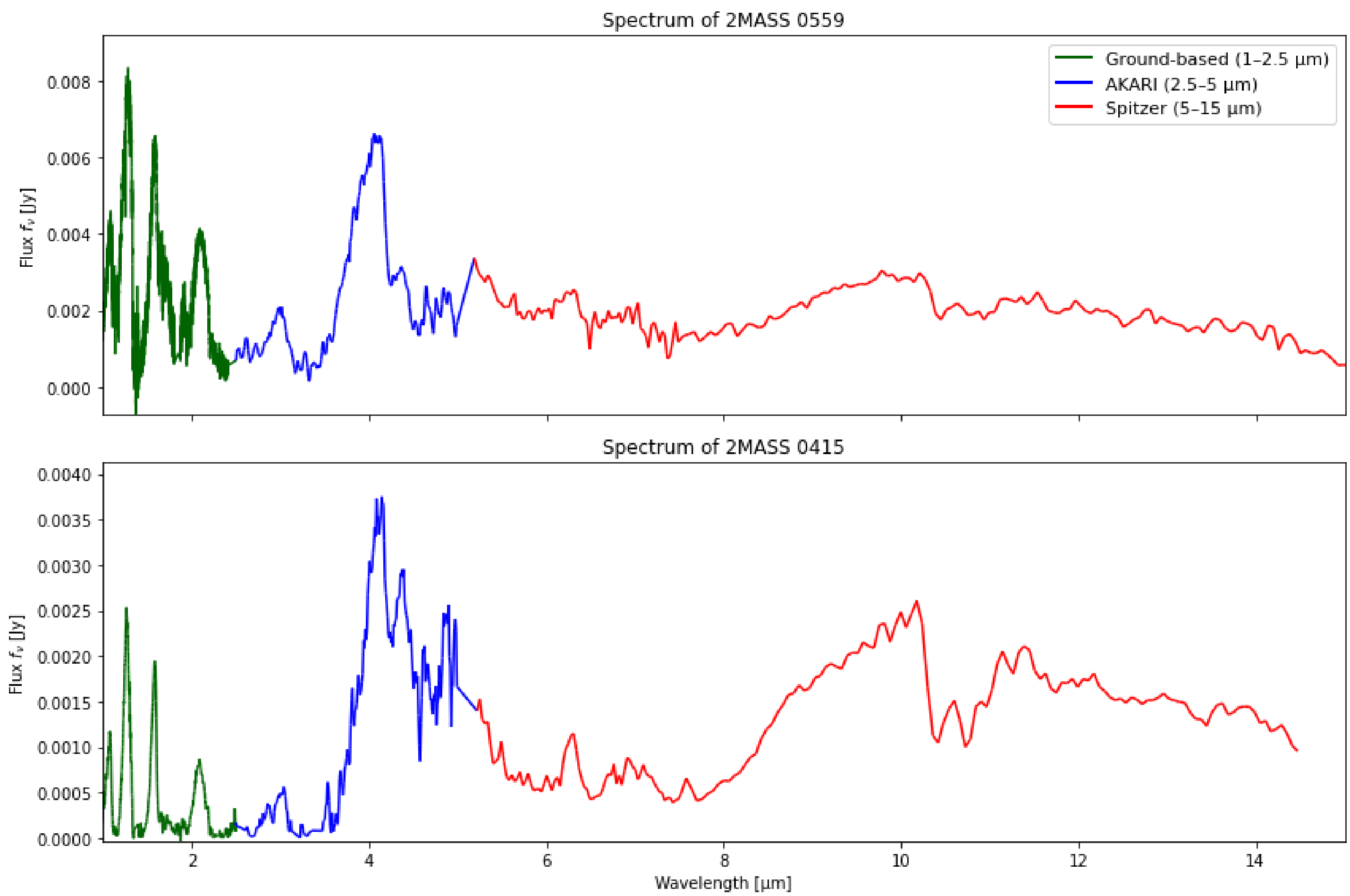

Figure 4.3 The 1-15 µm spectrum of 2MASS 0559 (top) and 2MASS 0415 (bottom) plotted. These spectra consists of ground-based observations (green), AKARI observations (blue), and Spitzer observations (red). Note that for visual purposes, a straight line was added when there were gaps between the ground and AKARI spectra as well as between the AKARI and Spitzer spectra.

4.2 Spectral Fitting Code

To find a best-fit model to the spectrum of a brown dwarf, we used a Python fitting algorithm (Turner et al. 2025) to read in the spectrum of a given brown dwarf and then iteratively find one of many atmospheric models from a given forward model library. We will refer to this code as the Python fitting algorithm.

The Python fitting algorithm allows its user the option to choose whether they want to fit a single spectral model or binary spectral model to the spectrum of a brown dwarf. In the case of the single fit, the code finds the best-fit model for the spectrum with the assumption that the brown dwarf is the only substellar object in its system. The binary fit operates under the assumption that a given brown dwarf is part of an unresolved substellar binary system and assumes that each component of the unresolved binary contributes to the total flux.

In each case, single and binary, the Python algorithm employs the use of adapted chi-squared analysis (Cushing et al. 2008) to find the best-fit model to the spectra of each brown dwarf to estimate effective temperature, cloud structure, gravity, and the extent of vertical mixing for each target. For 2MASS 0415 there is no evidence that it may be a binary system (Burgasser et al. 2006a). In contrast, 2MASS 0559 is suspected to be a binary system due to over-luminosity. Despite the binary potential, a single-fit was found to be sufficient in modeling its 1-15 µm spectrum.

For each object's data set, we fit individual subsections of each spectrum and the spectrum as a whole (i.e., 1-2.5 µm, 2.5-5 µm, 5-15 µm, and 1-15 µm) to the Sonora models to compare the impact of each wavelengths. One reason for this is that we suspect that different parts of the atmosphere are being probed at different wavelengths. Additionally, there are different resolution and different amounts of flux in each spectral region. The results of using the spectral fitting code to find the best-fit model using the Sonora forward models is summarized in Tables 4.1 and 4.2.

Due to the cool temperatures and noticeable disequilibrium features at 4.6 µm and 10.3 µm in the spectra of 2MASS 0415 and 2MASS 0559, it was anticipated that many, if not all, of the best model fits using the Sonora family would come from the Cholla models that incorporated disequilibrium chemistry. This expectation was borne out, with the best-fitting models consistently drawn from the Cholla grid.

As we look further into Tables 4.1 and 4.2, there are a few patterns to note. The highest temperature in the best-fit model for 2MASS 0415 came from the 2.5-5 µm range. Additionally, the lowest best-fit temperature came from the 1-2.5 µm range. There are two possible reasons that we see different temperatures for each best-fit at different wavelengths. The first reason may be that different wavelengths are probing different parts of the atmosphere. This would result in a continuum that is higher than expected in the 2.5-5 µm range as the flux from deeper within the atmosphere penetrates to the upper atmosphere. Additionally, when we also see a lot of vertical mixing in a brown dwarf's spectrum, that produces an overabundance of CO, which will result in a model with a higher value for temperature and K_{zz} being the best fit.

2MASS 0559 does not show any statistical difference for the values in the best-fit parameters (i.e., temperature, K_{zz}, etc.) and all best-fit values are within errors, with the exception of K_{zz} of 7 for 1-2.5 µm.

Table 4.1 This table presents the best-fit forward model using the Sonora model libraries for 2MASS 0415.

Forward Model Results for 2MASS 0415				
	Model Library	Temperature (Kelvin)	Gravity (log) (cgs)	Vertical Mixing (K_{zz})
1–15 µm	Cholla	750	4.25	2
1–2.5 µm	Cholla	800	4.25	4
2.5–5 µm	Cholla	1000	5.5	2
5–15 µm	Cholla	850	4.25	2

Table 4.2 This table presents the best-fit forward model using the Sonora model libraries for 2MASS 0559.

Forward Model Results for 2MASS 0559				
	Model Library	Temperature (Kelvin)	Gravity (log) (cgs)	Vertical Mixing (K_{zz})
1–15 µm	Cholla	1300	5.5	4
1–2.5 µm	Cholla	1200	4.75	7
2.5–5 µm	Cholla	1300	4.5	4
5–15 µm	Cholla	1250	4.5	2

In Figures 4.4 and 4.5, we display the observed spectrum of 2MASS 0415 and 2MASS 0559 in black with the best fitting Cholla model in red from 1-15 µm. In Figure 4.4, we find that the best-fit Cholla model does a good job of modeling the CO absorption feature at 4.6 µm for 2MASS 0415. On the other hand, we see that the depth of NH_3 is slight over-fit and the CO_2 feature at 4.2 µm is significantly under-fit. There is also some under- and over-fitting in the near-infrared. Particularly, we see over-fitting in the J-band peak and under-fitting in the H- and K-band peaks. Looking at the residual plot at the bottom of Figure 4.4, we see that the largest disagreement between the model and spectrum of 2MASS 0415 occurs around the 4 µm peak, where the model cannot fit. The current theoretical models require a non-physical C/O to fit this feature (Beiler et al. 2024b).

For 2MASS 0559, Figure 4.5 showcases the worst fitting by the best-fit Cholla model occurs when modeling CO_2, despite the CO_2 absorption feature not being as strong as what we see in 2MASS 0415. We also see over-fitting in the J-band peak and under-fitting in the H- and K-band peaks. The best-fit Cholla model for 2MASS 0559 only slightly under-fits the CO absorption feature at 4.6 µm. As we saw in 2MASS 0415, the models cannot replicate the depth of the CO_2 absorption feature. Overall, CO, CH_4, and NH_3 were well-fit at the expense of the near-infrared.

In addition to outputting the best-fit parameters, the spectral fitting code produces a heat-map that showcases the temperature and gravity ranges for the top 200 best-fit models. Figure 4.6 highlights the heat-map for 2MASS 0415 using the Sonora grid of models from 1-15 µm. The darker colors correspond to a solution that was found more often than others. Therefore, the darker colors are the most probably temperatures. The purpose of the heat-map is to provide uncertainties for temperature, and to showcase that gravity is not well-constrained. Using the uncertainties for temperature allows us to know by how much we can adjust this parameter in PICASO before creating a model with higher error. Similarly, Figure 4.7 highlights the heat-map for 2MASS 0559 using the Sonora family of models from 1-15 µm and we extract information about temperature to help us create accurate models in PICASO. For 2MASS 0415, temperature is tightly constrained, but gravity is not. We see this because the best chi-squared values are within a narrow temperature range. For 2MASS 0559, there are two best-fit temperature regions around 1100 K and 1200 K. For both 2MASS 0415 and 2MASS 0559, gravity is not constrained which is typical for brown dwarfs.

4.3 PICASO Fitting

PICASO is an interactive hybrid forward model that allows us to change parameters to try to better fit the 1-15 µm spectrum of 2MASS 0415 and 2MASS 0559. With PICASO, I can create a simple temperature-gravity model, a chemical equilibrium model, and a chemical disequilibrium model. The default flux for PICASO models are f_λ and are in units of ergs/cm^2/sec/cm. Since the units of flux for 2MASS 0415 and 2MASS 0559 were in Janskys, it was decided after experimentation that converting PICASO's model flux units was the best course of action.

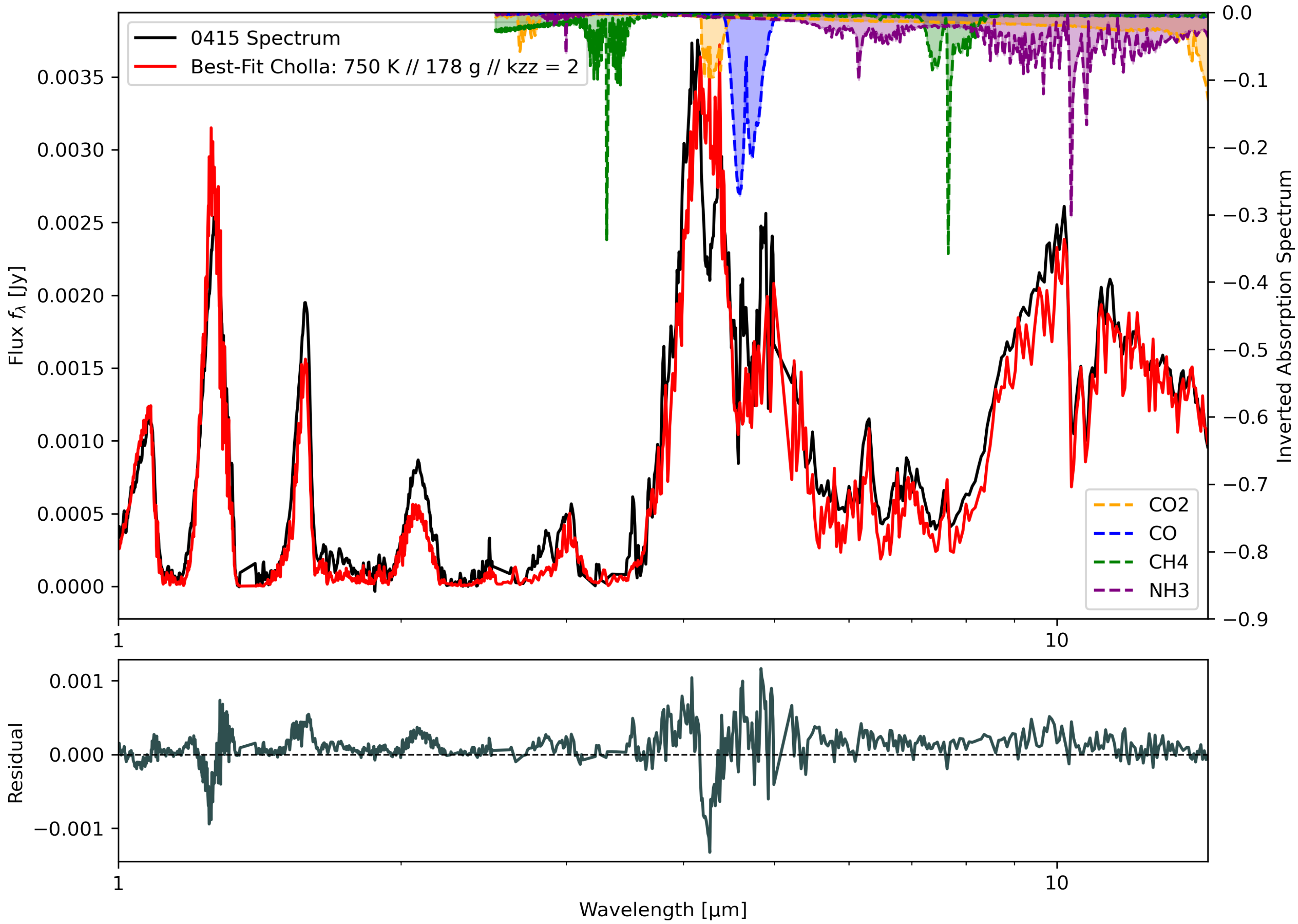

Figure 4.4 Spectrum of 2MASS 0415 from 1-15 μm (black) and best-fit Cholla forward model (black). The inverted absorption spectra of CO_2, CO, CH_4, and NH_3 from NIST are plotted as dotted lines in differing colors. We highlight the CH_4 absorption feature around 8 μm and the NH_3 absorption feature seen in the 10 μm band.

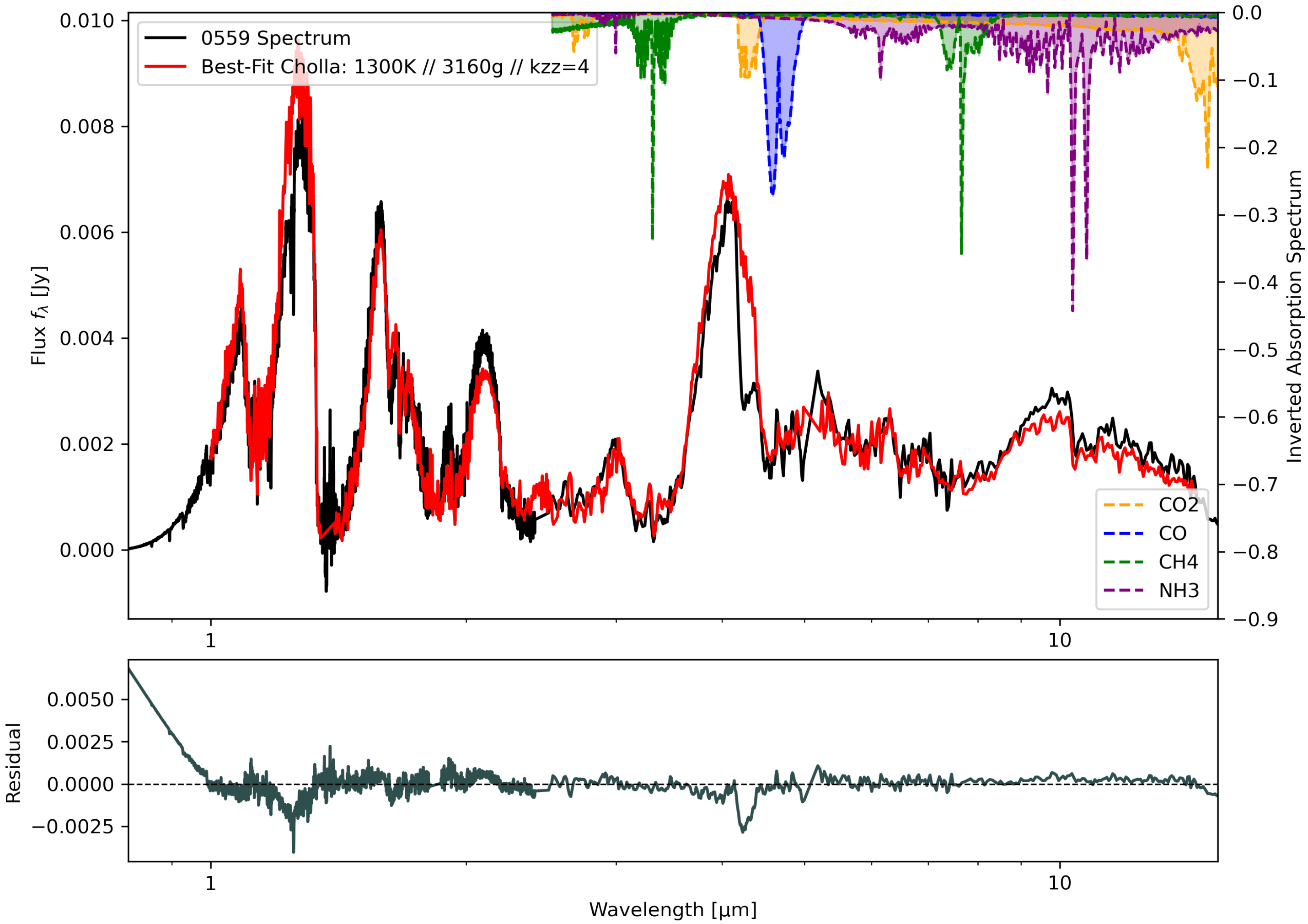

Figure 4.5 Spectrum of 2MASS 0559 from 1-15 µm (black) and best-fit Cholla forward model (black). The inverted absorption spectra of CO_2, CO, CH_4, and NH_3 from NIST are plotted as dotted lines in differing colors. We highlight the CH_4 absorption feature around 8 µm and the NH_3 absorption feature seen in the 10 µm band.

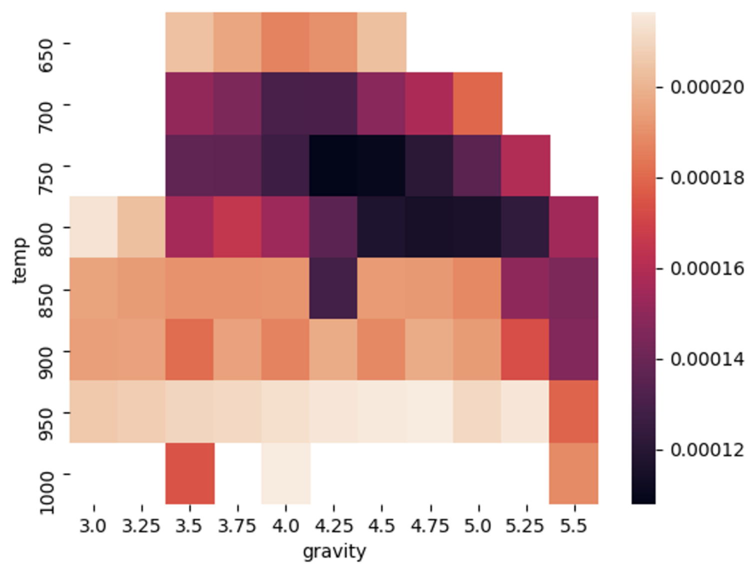

Figure 4.6 Heat-map plot for the 200 best-fit Sonora models for 2MASS 0415 for the 1-15 µm range. The darker colors correspond to lower χ^2 values. These weighted chi-squaredχ^2 values are on the right side of the y-axis. We know that temperature is well-constrained as the temperatures with lower χ^2 values are marked in dark purple and black, and are clustered around 750 K. On the other hand, we see that gravity is not well-constrained because there is a wide range of gravity values that have lower χ^2 values.

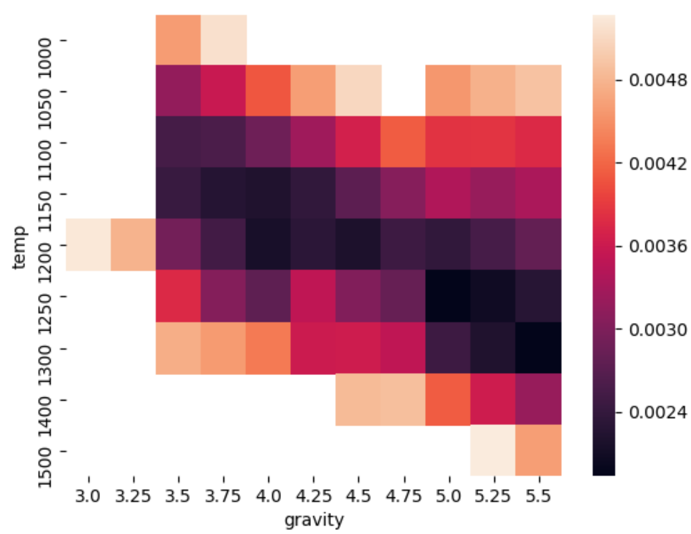

Figure 4.7 Heat-map plot for the 200 best-fit Sonora models for 2MASS 0559 for the 1-15 μm range. The darker colors correspond to lower χ^2 values. These weighted chi-squaredχ^2 values are on the right side of the y-axis. Temperature values for 2MASS 0559 is less constrained than what was seen in Figure 4.4 for 2MASS 0415. Just like with 2MASS 0415, gravity is also poorly constrained.

To use PICASO to create any sort of model, whether it be a simple temperature-gravity model or a more complex model such as one with clouds of varying species, I used PICASO's given opacity file that could cover the 1-15 µm range. An opacity file contains information on absorption coefficients on 20 to 30 of the expected molecules for a given pressure and temperature layer in the atmosphere. When creating an atmospheric model, the molecular opacity defines how likely a photon at a given wavelength will have an interaction with a given molecule at each layer of the atmosphere. The molecular opacity file tells us which percentage of photons are being observed or scattered. Creating a good-quality opacity file can be done via a tutorial by Mukherjee et al. (2022). Opacity files are created using the correlated-k approach in which the opacity is vertically correlated to more accurately capture differing layers of a brown dwarf's atmosphere.

For this project, I began by creating a simple temperature-gravity model to familiarize myself with how PICASO generates a model. Following a PICASO tutorial (Mukherjee et al. 2022), I used the best-fit temperature and gravity for 1-15 µm to make a model for 2MASS 0415 (as seen in Table 4.1). This process is replicated for 2MASS 0559. Figures 4.8 and 4.9 showcase simple temperature-gravity model fits to the spectra of 2MASS 0415 and 2MASS 0559, respectively, that are then improved on later by adding vertical mixing. In the aforementioned figures, we see that there is an over-prediction of CO at 4.6 µm and an under-prediction of NH_3 at 10.3 µm for 2MASS 0415 and 2MASS 0559 because disequilibrium chemistry is not included.

Taking a closer look at 2MASS 0415, in Figure 4.8, we see significant under-fitting in the 5-15 µm region, along with over-fitting in the 4-5 µm range. We do find that a simple model does a fair job at modeling the 1-2.5 µm region, but we can visually conclude that a more complex model will more accurately model the molecular absorptions features of 2MASS 0415.

For 2MASS 0559, in Figure 4.9, we find that the near-infrared only has slight over-fitting, but the mid-infrared is not well-modeled using the simple model. In particular, we see that there is over-

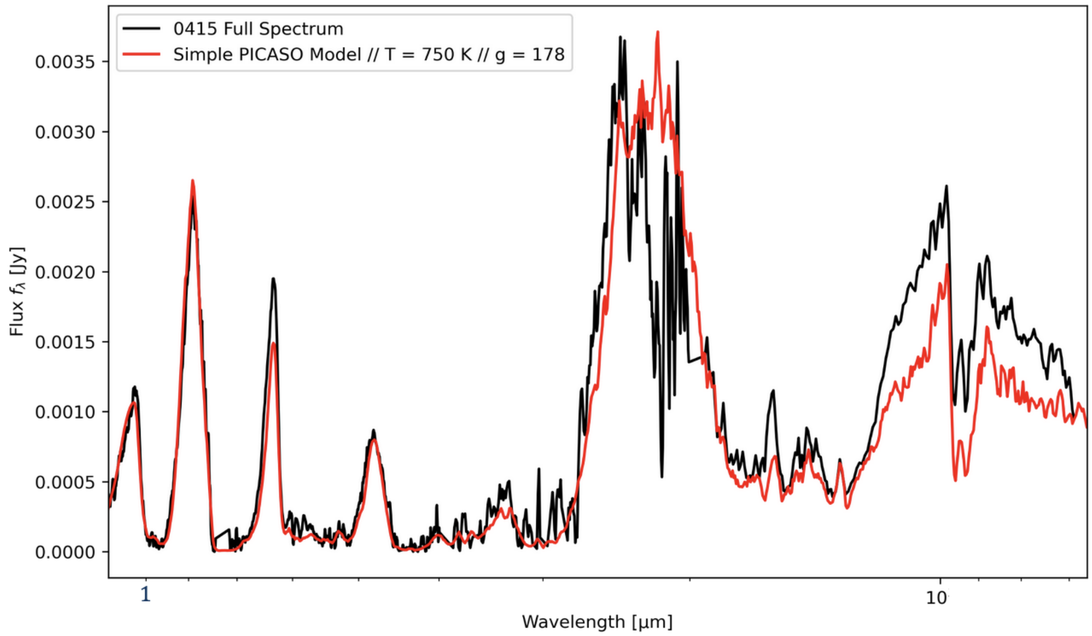

Figure 4.8 The 1-15 µm spectrum (black) for 2MASS 0415 and a simple temperature-gravity model (red) using PICASO. This model does not include any vertical mixing, no C/O, and no metallicity – this is the most basic model.

and under-fitting in the 4-5 µm region, and under-fitting in the 5-15 µm range. Like with 2MASS 0415, a more complex model is needed to better model the spectrum of 2MASS 0559.

For both 2MASS 0415 and 2MASS 0559, a simple model underestimates the amount of CO at 4.6 µm in the upper atmosphere and it cannot replicate the continuum and the depth at the same time of NH_3 at 10.3 µm. In order to explain the CO, we need to introduce a more complex model by including vertical mixing.

To replicate the strength of the CO band at 4.6 µm, we need to introduce chemical disequilibrium into the model, but to start, I created a chemical equilibrium model. To include chemical equilibrium, PICASO solves for the atmospheric structure of brown dwarfs, which includes making an initial guess on the temperature-pressure profile, the chemical structure, and the energy transport in the atmosphere. These three structures are not independent of each other, since the chemistry is dependent on the temperature-pressure profile and the radiative transfer depends on the molecular

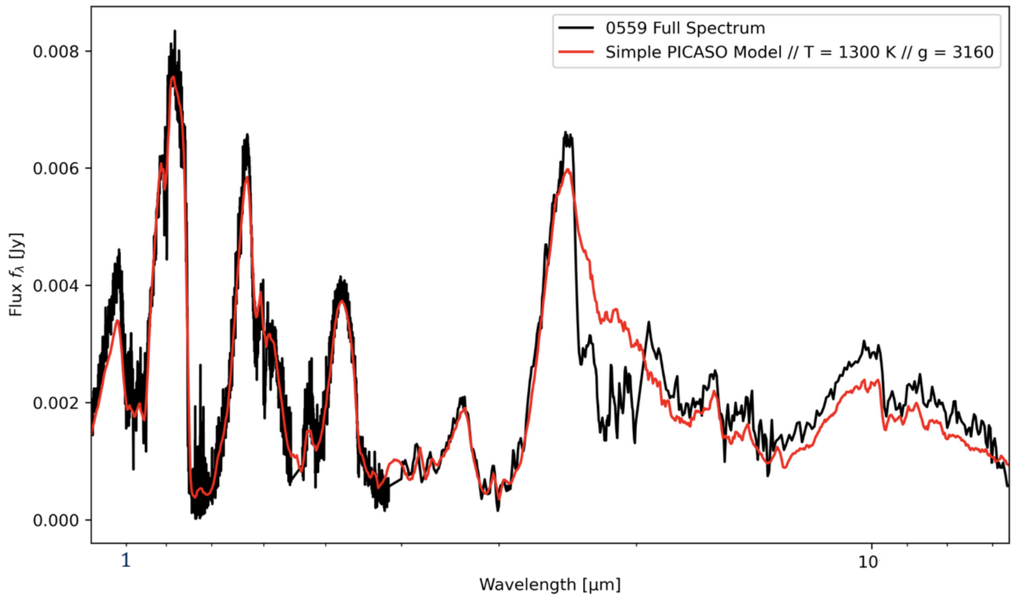

Figure 4.9 The 1-15 µm spectrum (black) for 2MASS 0559 and a simple temperature-gravity model (red) using PICASO. This model does not include any vertical mixing, no C/O, and no metallicity – this is the most basic model.

opacity. PICASO works to find the atmospheric state of a brown dwarf by accounting for these processes and their connections to one another self-consistently and iteratively. In creating the chemical equilibrium model, Mukherjee et al. (2022) recommends that the number of layers in the model should be between 51-91. We chose to include 91 pressure layers for creating our chemical equilibrium models.

Two new parameters are introduced in investigating chemical equilibrium and they are as follows: **nofczns**, which is the number of convective zones, and **rfacv**, which is the total net radiative flux in the nth atmospheric layer. Equation 4.1 taken from Mukherjee et al. (2022) shows how `rfacv`, which is represented by F^n_{net} is calculated. The layered radiative-flux is defined as:

$$F^n_{net} = r_{th} F^n_{thermal,net} \tag{4.1}$$

where F represents the flux, which in this case is accounting for net and thermal flux, and r_{th} is the contribution factor of the thermal radiation to the net flux, which is generally fixed at a value of one. The only cases in which r_{th} is not equal to one would be if there are non-thermal contributions or when accounting for non-local thermal equilibrium. The tutorial sets more parameters that are kept fixed for creating chemical equilibrium models (Mukherjee et al. 2022).

A chemical disequilibrium model (Mukherjee et al. 2024) is created by including the eddy diffusion constant, K_{zz}, which represents the strength of vertical mixing. The two settings for K_{zz} are as follows: a constant value that is set at every atmospheric layer, or a self-consistent value using equations 4.2 and 4.3 from Mukherjee et al. (2022) that calculate a value for each layer based on temperature and pressure.

$$K_{zz} = \frac{H}{3}\left(\frac{L}{H}\right)^{4/3}\left(\frac{RF}{\mu\rho_a c_p}\right)^{1/3} \tag{4.2}$$

$$K_{zz} = \frac{5\times 10^8}{{P_{bar}}^{1/2}}\left(\frac{H}{620km}\right)\left(\frac{T_{eff}}{1450K}\right)^4 \tag{4.3}$$

In Equations 4.2 and 4.3, H is the local scale-height of the atmosphere, L is the turbulent mixing length, R is the universal gas constant, μ is the mean molecular weight, ρ_a is the atmospheric density, c_p is the atmospheric specific heat at constant pressure, P_{bar} is the pressure measured in bars, and F is the convective heat flux. Both of these equations can be found in the **get kzz** function in PICASO. Essentially, as the temperature profile iterates towards the converged solution, the fixed levels of various gases change. This results in the abundance of quenched species to depart from chemical equilibrium (Mukherjee et al. 2022).

The chemical disequilibrium model is different from that of the chemical equilibrium model in that six new parameters are introduced. These parameters are as follows: **diseq chem** that is set to true, which turns on disequilibrium chemistry; **self-consistent kzz**, which can be set to true or false to solve self-consistently for K_{zz}; **save all kzz**, which saves the intermediate K_{zz} values if

self-consistent kzz is set to true; **kzz**, which is a constant value if **self-consistent kzz** is set to false; **gases fly**, which determines the gases that are included in the climate calculation; and **chemeq first**, which converges a chemical equilibrium model first. Of these six new parameters, the user is likely to only change **kzz** and may have the desire to experiment with **self consistent kzz** versus **constant profile**. Mukherjee et al. (2024) recommend that **gases fly** remains unchanged, which we follow for this project. The gases in **gases fly** include: CO, CH_4, H_2O, NH_3, CO_2, N_2, HCN (hydrogen cyanide), H_2 (molecular hydrogen), PH_3 (phosphine), C_2H_2 (ethyne), Na, K, TiO (titanium oxide), VO (vanadium oxide), and FeH (iron hydride).

Values of **kzz** were varied between the following values: 1, 2, 4, and 7, with larger values indicating that there is greater amounts of mixing. We also varied the values of C/O and metallicity. The C/O values that we used to compute disequilibrium models ranged from: 0.25, 0.50, 1.0, 1.5, 2.0, and 2.5. The metallicity values that we used to compute disequilibrium models ranged between -1 and 1 with steps of 0.5.

The best fits from including vertical mixing are seen in Figure 4.4 and Figure 4.5. A more thorough discussion on the best disequilibrium model fits will be given in Chapter 5. It can be seen that including vertical mixing results in a better-fit model than using a simple model (see Figures 4.8 and 4.9), and we can especially see that the CO feature at the 4.6 μm band and NH_3 at the 10.3 μm band are better represented when accounting for vertical mixing.

Chapter 5

Results

This chapter contains the results of the best-fit PICASO disequilibrium models to 2MASS 0415 and 2MASS 0559. This chapter is split into two sections, each examining the best-fit models of the 1-15 μm spectrum of 2MASS 0415 and 2MASS 0559, respectively. Each section of this chapter discusses trends seen in varying the extent of vertical mixing, C/O abundances, and metallicity. We investigate how varying one parameter changes model fits with respect to the observed spectrum so that we can better understand which parts of the brown dwarf's spectrum are sensitive to specific parameters. This chapter also includes a discussion on how these results compare to prior studies that have looked to explore the characteristics of 2MASS 0415 and 2MASS 0559 in different spectral ranges.

To create a best-fit model of a brown dwarf spectrum using PICASO, we used the parameters from the best-fit Cholla model as a starting point for temperature and gravity. Values of the eddy diffusion constant, K_{zz}, along with the C/O abundance ratio and metallicity were varied in an effort to find a model that would accurately model the CO, CH_4, NH_3, and CO_2 absorption features seen in the 1-15 μm spectra of 2MASS 0415 and 2MASS 0559. Beiler et al. (2024a) have shown that metallicity and C/O ratio has an impact on abundances of CO and CO_2. As the numerical value of C/O increases, we expect to see a higher abundance of CO and CO_2 in the atmosphere, which can be seen by the increasing depth of those molecular absorption features.

The use of adapted chi-squared fitting was employed to calculate the best-fit model for 2MASS 0415 and 2MASS 0559 (Cushing et al. 2008). Equation 5.1 was used to calculate the best scale factor (C_k) and chi-squared value (G_k). C_k is the radius of a brown dwarf squared divided by the distance of the brown dwarf squared. When calculating the adapted-chi squared, we are taking all of the data points (f_i) and subtracting each point from the model spectrum flux (F) times C_k, which is scaling the flux for distance. By doing so, we are adjusting the scale C_k so that subtracting the model flux from the data flux yields the smallest residuals. σ_i is the error of the flux values. Note that i is each individual data point. Weighting (w_i) was used to account for the different resolution of the observations used to create the final spectrum.

Since the 1-15 µm spectrum contained data of varying resolution, the weights (w_i) for the ground, AKARI, and Spitzer data were adjusted such that the AKARI and Spitzer spectrum carry an equal weight to the ground-based spectrum when fitting. The ground-based data has a resolution of 2000, whereas the resolution for AKARI and Spitzer is 120 and 90, respectively. In particular, we see that the ground-based data has 1752 data points, the AKARI data has 216 data points, and the Spitzer data has 192 data points.

$$G_k = \sum_{i=1}^{n} w_i \left(\frac{f_i - C_k F_{k,i}}{\sigma_i} \right)^2 \tag{5.1}$$

5.1 2MASS 0415 PICASO Best-Fit Model

For 2MASS 0415, the weights for the 1-2.5 µm data was set to 0.0004, 2.5-5 µm was set to 0.01, 5-15 µm was set to 0.1. These weights were experimentally chosen based on the flux of the brown dwarf. We set the weights until it was apparent that each spectral region was able to contribute to the spectral fit. In this fitting we did not have error values (σ_i) for the flux of 2MASS 0415, because when 2MASS 0415's 1-2.5 µm spectrum was reduced and processed in the early 2000s, the errors were not included as they were deemed to be significantly smaller than the flux. As such, the value of σ_i was set to 1 for all wavelengths. Table 5.1 lists the chi-squared values for the best-fit models for 2MASS 0415, along with the chi-squared values of other models where parameters are slightly varied.

The best-fit PICASO model to the 1-15 μm spectrum of 2MASS 0415, along with the corresponding residual plot, is presented in Figure 5.1. The parameters of the best-fit model are as follows: T_{eff} = 750 K, g = 178 m/s^2, K_{zz} = 2, C/O = 1.0, and [M/H] = 0.

The best-fit model for 2MASS 0415 is successful in modeling the CO feature at 4.6 μm, along with the NH_3 feature at 10.3 μm. The 1-2.5 μm region is generally well-fit, with minor under- and over-fitting in the J-, H-, K- bands. The best-fit model does a good job of modeling the near- and mid-infrared. As seen in the residual plot on the bottom panel of Figure 5.1, we fail to fit the CO_2 at 4.2 μm and we slightly over-fit the CO band at 4.6 μm. We find that no amount of varying C/O can fit the CO_2 features, which tells us that some fundamental physics is missing from the models (Beiler et al. 2024b).

Table 5.1 This table summarizes how reduced χ^2 values of alternative models compare to the χ^2 value of 2MASS 0415's best-fit model. The best-fit model of 2MASS 0415 is highlighted in bold with double lines underneath. Each row afterwards showcases how χ^2 values differ when varying atmospheric parameters by one step. Each of the models presented in this table are plotted and compared to each other throughout this chapter.

Model	**Temperature (K)**	**log(K_{zz})**	**C/O**	**Reduced χ^2**
Best Fit	**750**	**2**	**1.0**	**4.21×10^{-4}**
Increase Temperature	800	2	1.0	4.20×10^{-4}
Decrease Temperature	700	2	1.0	5.48×10^{-4}
Increase log(K_{zz})	750	4	1.0	6.48×10^{-4}
Decrease log(K_{zz})	750	1	1.0	4.36×10^{-4}
Increase C/O	750	2	1.5	6.0×10^{-4}
Decrease C/O	750	2	0.5	4.24×10^{-4}

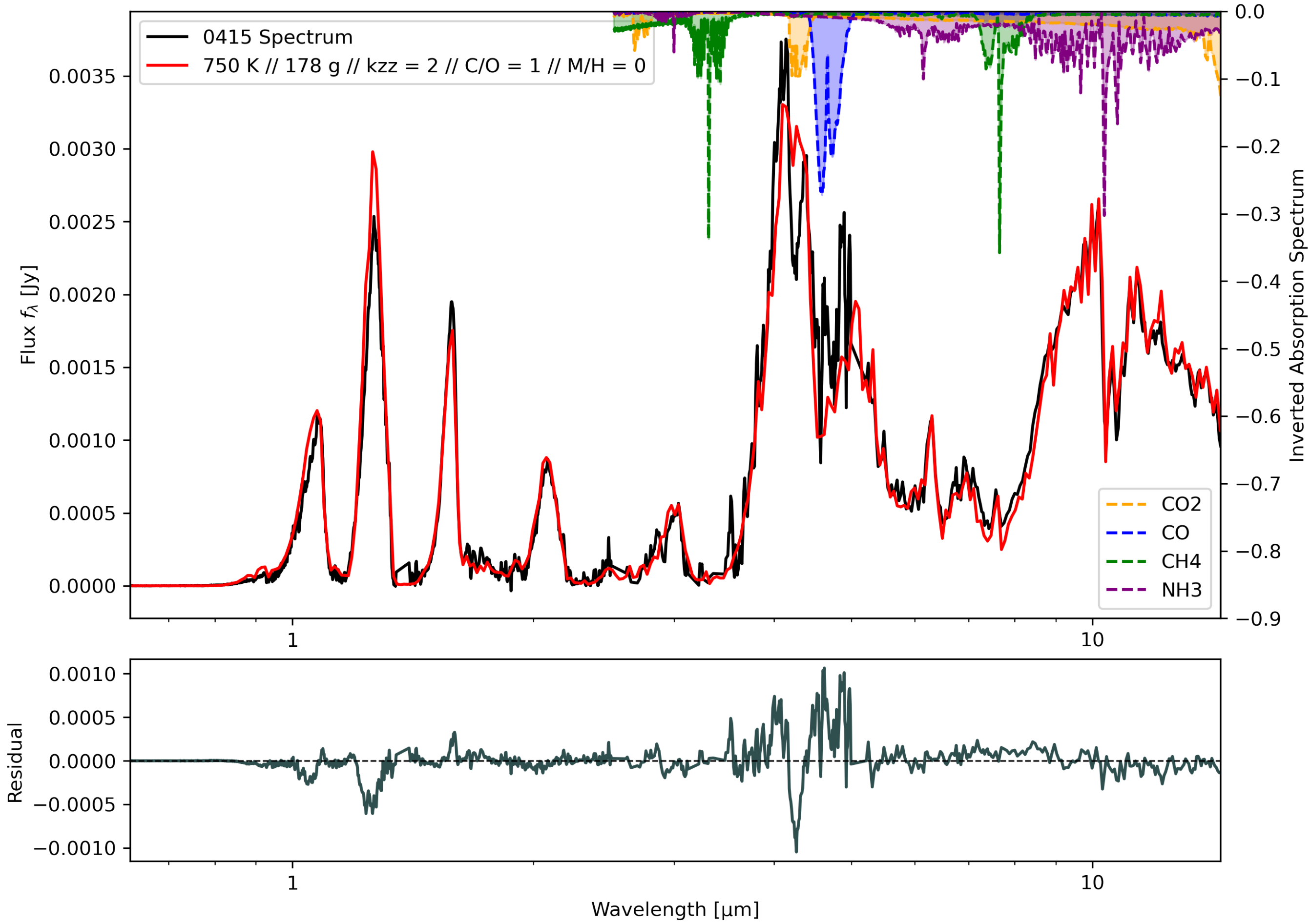

Figure 5.1 Plotted is the 1-15 μm spectrum for 2MASS 0415 (black) along with the best-fit PICASO disequilibrium model (red). Plotted invertedly on top is the absorption spectrum of CO_2 (orange), CO (blue), CH_4 (green), and NH_3 (purple). Here we see that the CO feature at 4.6 μm and the NH_3 feature at 10.3 μm is accurately modeled, but the depth of the CO_2 absorption feature is not well-modeled. Plotted beneath the best-fit model is the residual between the best-fit model and the spectrum, which highlights regions where there is over- and under-fitting.

Varying temperature of the best-fit model by ±50 K, even if all other parameters are fixed, gives us some sense for which spectral features are sensitive to temperature, which is seen in Figure 5.2. At 750 K, the best-fit model does a good job of modeling the 2.5-15 μm spectrum, with minimal over- and under-fitting in the 1-2.5 μm spectrum. While the models at 700 K and 800 K do not fit the near-infrared as well. The data is still well-fit at 2.5-15 μm, suggesting that these regions are not as sensitive to effective temperature as 1-2.5 μm. We find that varying temperature does not improve the poor fit to CO_2. The input of temperature on fitting CH_4, CO, and NH_3 is minimal and those are largely unaffected by small temperature changes.

Statistically, the models with temperatures at 750 K and 800 K both yielded very similar χ^2 (chi-squared) values. While the model at 800 K has a slightly better χ^2, we found through visual inspection that the model at 750K has a better fit to the 1-2.5 μm region without significant over- or under-fitting in the mid-infrared. Additionally, a best-fit model of 750 K is also in more agreement with other studies that have looked to characterize the atmospheric properties of 2MASS 0415.

The next steps in this analysis involved exploring how K_{zz} and C/O affect the model fits to 2MASS 0415. Since surface gravity is a poorly constrained parameter (Stephens et al. 2009), we did not explore the variations of gravity. Additionally, we found that varying metallicity did not lead to significant changes in model fits. In particular, sub-solar and super-solar metallicities did not improve model fits.

Figure 5.3 showcases how changing values of vertical mixing affects models fits. With temperature fixed at 750 K and vertical mixing values of 1, 2, and 4, it can be seen that changing the extent of vertical mixing has little affect on how well the models fit from 1-2.5 μm and the NH_3 absorption feature at 10.3 μm. The main difference that can be seen is how well the CO feature is modeled. While CO should not be prevalent at 750K, vertical mixing causes there to be a deeper CO feature in this cooler atmosphere. Increasing K_{zz} increases the depth of the CO absorption feature and it was found by eye and statistically, that a K_{zz} value of 2 best models CO, along with NH_3. Increasing

K_{zz} also leads to a statistically worse fit (see Table 5.1). One clear takeaway from Figure 5.3, is that the 3-5 μm region in 2MASS 0415 is very sensitive to K_{zz}. Increasing and decreasing K_{zz} by two steps has a significant impact on the depth of CO and on the modeling of the 4 μm peak.

Despite the changes in K_{zz}, none of the models are able to accurately model the CO_2 feature in the 4.2 μm band. This could be an indication that vertical mixing does not play a significant role in the appearance of CO_2 in the upper atmosphere, and the prescence of this molecule may be driven by abundances of metals, such as carbon and oxygen, or that the models are missing critical C/O chemistry.

Values of C/O were varied to see how changing C/O in PICASO affects modeling key absorption features (CO and CO_2) seen in the 2MASS 0415 spectrum. Figure 5.4 plots models with C/O values of 0.5, 1, and 1.5. While changing C/O does show small changes in the modeling of CO, its affects are not as prominent as those from vertical mixing. While increasing C/O slightly improves the fit to CO_2, this absorption feature is still significantly under-fit. Beiler et al. (2024b) noted a similar under-fitting of CO_2 in their sample of late T- and Y-dwarf atmospheres and found that CO_2 could only be well-modeled using unrealistic values of C/O and metallicity. Table 5.1 further shows, statistically, that increasing C/O creates a poorer fit to 2MASS 0415 compared to lower values of C/O.

In Saumon & Marley (2008)'s study of the atmospheric properties of two cool T-dwarfs, one of which included 2MASS 0415, they used spectra from Spitzer and ground-based telescopes for their analysis. Using cloudless models, Saumon & Marley (2008) found the following best-fit parameters for 2MASS 0415, temperature ranged from 690 K to 775 K, gravity ranged from 479 m/s^2 to 2344 m/s^2, and K_{zz} ranged from 4 to 6. While values for temperature are in agreement with this study, they predicted much higher gravity and K_{zz} (Saumon & Marley 2008). This discrepancy is likely in part due to the addition of AKARI data from 2.5-5 μm and also because the understanding of substellar atmospheres has evolved along with the inclusion of various values for the C/O abundance and the metallicity. The large range of possible values for surface gravity occur because it is a poorly constrained parameter in all brown dwarfs.

A more recent study only analyzed 2.5-15 μm spectrum of 2MASS 0415 and 2MASS 0559 using Spitzer and AKARI (Mukherjee et al. 2024). For their analysis, they employed the use of the Sonora Elf-Owls to obtain best-fit parameters, which were calculated via interpolating the grid of the Sonora Elf-Owl models. Using the Elf-Owl model grid on the 2MASS 0415 2.5-15 μm spectrum, Mukherjee et al. (2024) found the following best-fit parameters (see Figure 5.5): T_{eff} = 737 K, g = 47 m/s^2, K_{zz} = 2.71, C/O = 0.18, and [M/H] = 0.11. Table 5.2 summarizes how Mukherjee et al. (2024)'s best-fit parameters compare to my PICASO results. There is close agreement in metallicity and temperature, while my predicted C/O from PICASO is higher than that of Mukherjee et al. (2024). Differences in surface gravity are negligible as surface gravity is poorly constrained. There is also slight differences in values of K_{zz}, which can be seen in how well both our results model the 4 μm peak, as seen in Figure 5.5. Differences in results can be attributed to the fact that we use 1-2.5 μm data in our fitting and Mukherjee et al. (2024) does not.

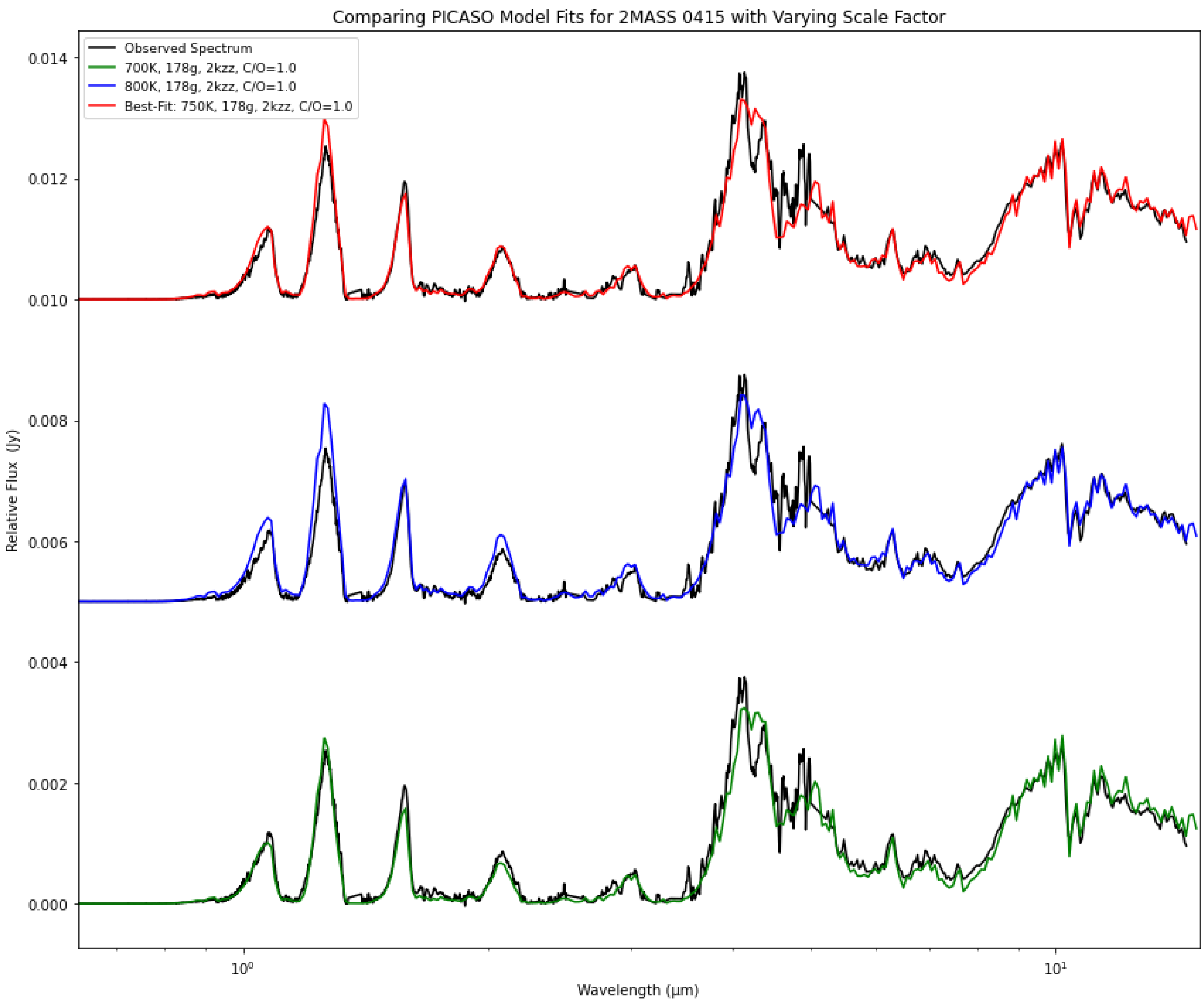

Figure 5.2 Plotted is the 1-15 μm spectrum for 2MASS 0415 (black) along with the best-fit PICASO disequilibrium model (red) and two models that share the same values for all parameters except for temperature. Each model is plotted with their corresponding scale factor.

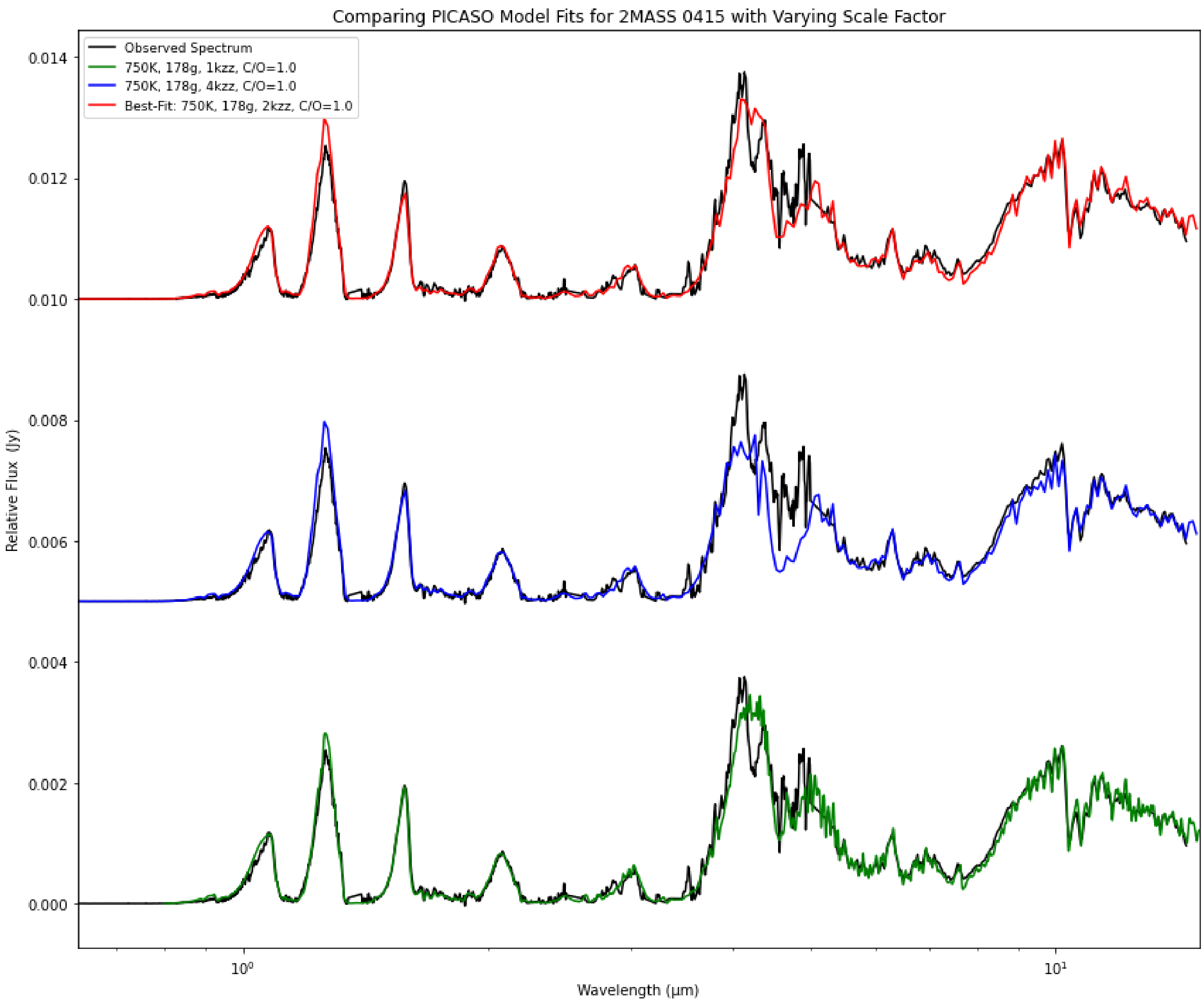

Figure 5.3 Plotted is the 1-15 µm spectrum for 2MASS 0415 (black) along with the best-fit PICASO disequilibrium model (red) and two models that share the same values for all parameters except for K_{zz}. Each model is plotted with their corresponding scale factor. While all values of K_{zz} accurately model NH_3, there is some variance in how well CO and CO_2 is modeled.

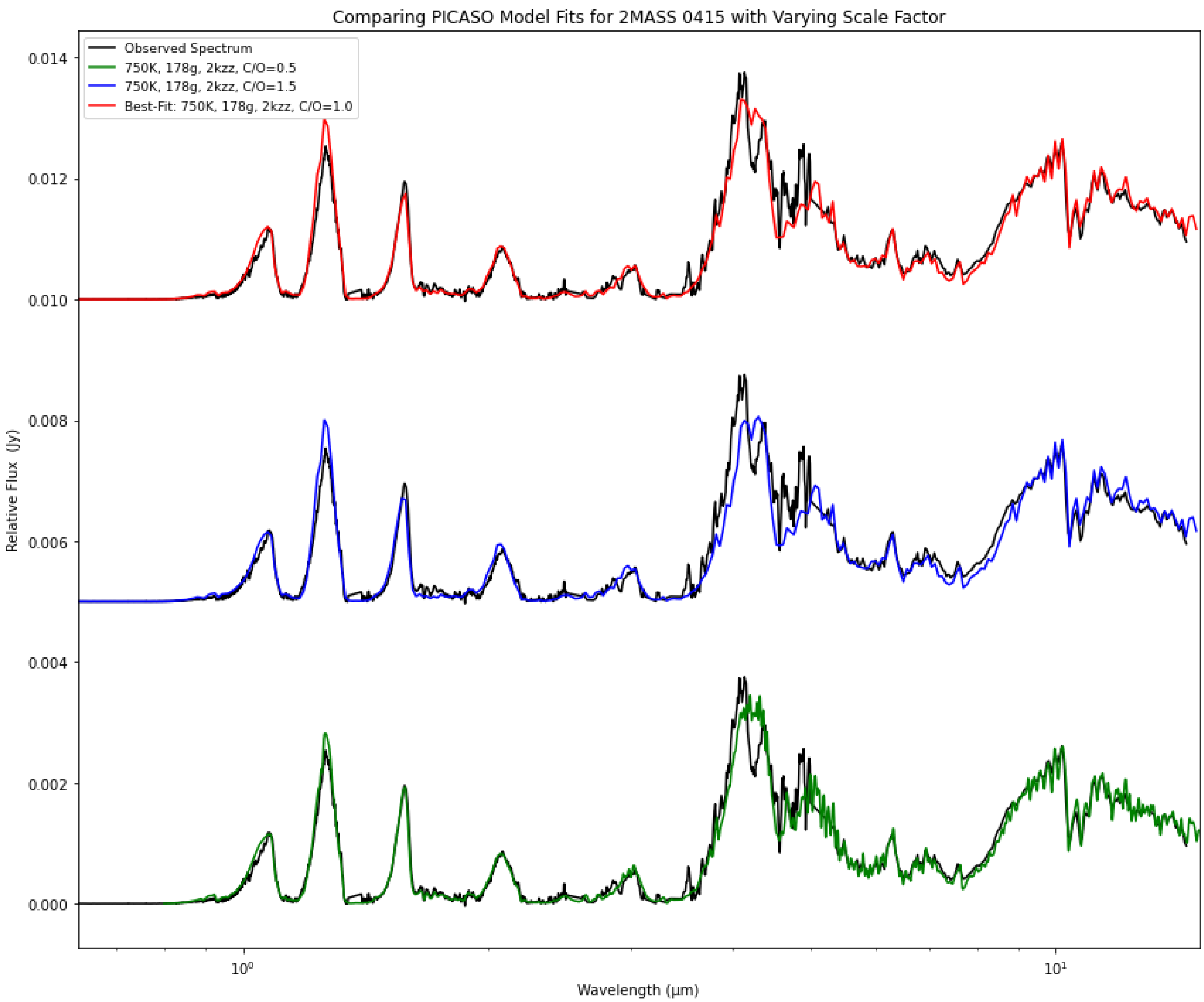

Figure 5.4 Plotted is the 1-15 μm spectrum for 2MASS 0415 (black) along with the best-fit PICASO disequilibrium model (red) and two models that share the same values for all parameters except for C/O. Even with each model being plotted with their corresponding scale factor, the effects of varying C/O is minimal.

Table 5.2 My best-fit PICASO and Mukherjee et al. (2024) 's best-fit Sonora Elf-Owls parameters to 2MASS 0415 across 1-15 µm and 2.5-15 µm, respectively.

Parameters from Best-Fit PICASO Disequilibrium Models for 2MASS 0415					
	Temperature (Kelvin)	Gravity (m/s^2)	Vertical Mixing (K_{zz})	C/O ratio	[M/H]
My PICASO best-fit	750	178	2	1.0	0
Mukherjee et al. (2024)'s best-fit	737	47	2.71	0.18	0.11

Figure 5.6 shows how this project's best-fit PICASO model of 2MASS 0415 compares to that of the Mukherjee et al. (2024) best-fit Elf-Owl model, which does not include ground observations from 1-2.5 µm. Our results and that of Mukherjee et al. (2024) yield good overall fits to 2MASS 0415's 1-15 µm spectrum, which minor differences in modeling some of the peaks in the near-infrared and the modeling of the 4 µm peak. Both models fail to model the CO_2 absorption feature, but do well to model the CO and NH_3 absorption features. Currently in our team, there is work being done to use PICASO and other forward models to model the 3-5 µm spectrum of 2MASS 0415 from JWST, which may yield more insight on some of the disparity seen in the best-fit model parameters.

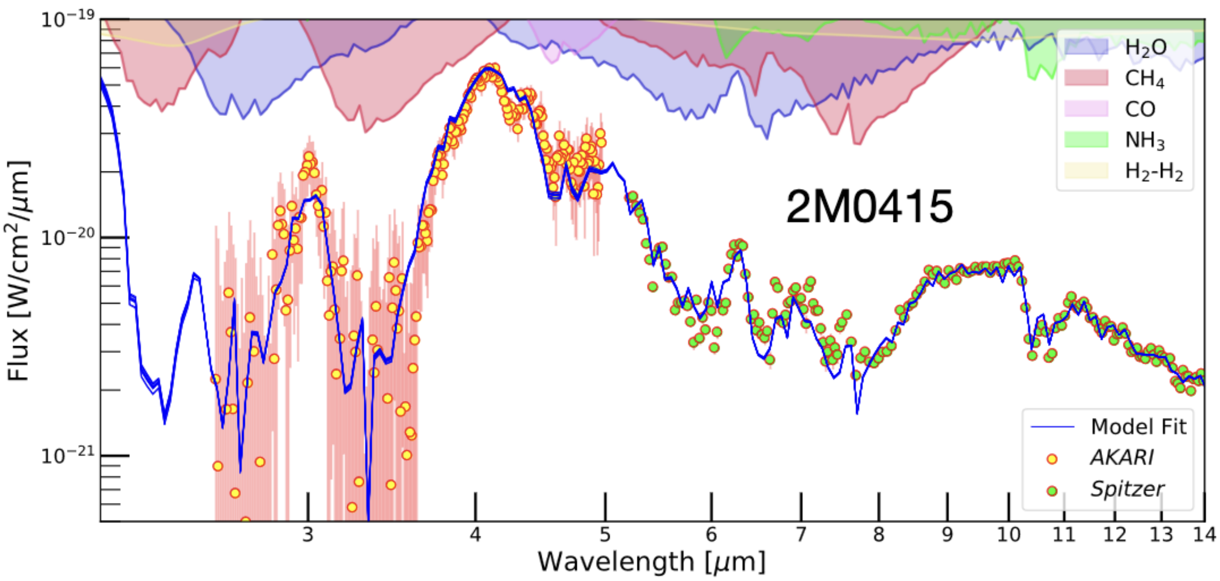

Figure 5.5 Best-fit Elf-Owl model to the 2.5-15 μm spectrum of 2MASS 0415 taken from Mukherjee et al. (2024). The spectrum from AKARI is represented by yellow circles and the spectrum from Spitzer is represented by green circles with the best-fit model in blue.

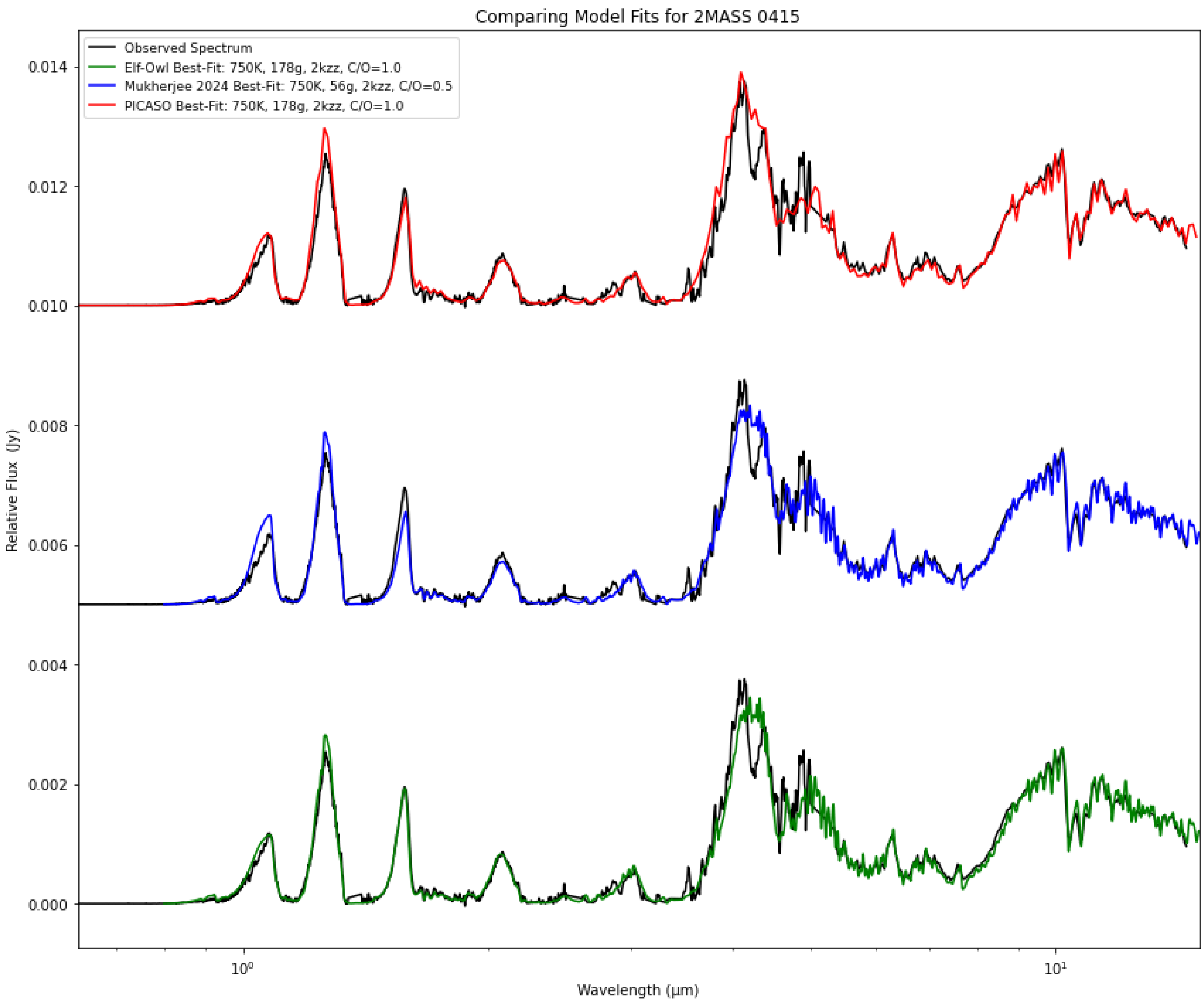

Figure 5.6 Plotted is the best-fit model of this project (red) plotted with the best-fit model from Mukherjee et al. (2024) (blue) along with the best-fit Elf-Owl model using this project's best fit parameters (green). The model fits to 2MASS 0415's 1-15 μm is in general agreement, although my best-fit model more accurately models the peak at 4 μm. None of the models are able to accurately model the CO_2 feature, but all models have good fits to CO and NH_3. The discrepancies in the model fit parameters may be attributed to the inclusion of 1-2.5 μm data in the analysis for this project.

5.2 2MASS 0559 PICASO Best-Fit Model

Next, we modeled the absorption features of the composite 1-15 μm spectrum of 2MASS 0559 in PICASO starting with the best-fit Cholla model results and then varying the parameters to find the best-fit PICASO model. Similar to the procedures in Section 5.1, we weighted different spectral ranges when calculating the χ^2 value of each model. Due to the fact that 2MASS 0559 is brighter in the near-infrared than 2MASS 0415, the values for the weights could not be the same. For 2MASS 0559, the weights for the 1-2.5 μm data was set to 0.001, 2.5-5 μm was set to 0.01, and 5-15 μm was set to 0.01. Additionally, χ^2 values for 2MASS 0559 vastly differ in order of magnitude compared to 2MASS 0415, because 2MASS 0559 has error values for each flux value that is measured, and the error along with the weights were not pulled out when calculating the final χ^2 value.

The best-fit PICASO model (see Figure 5.7) for the 1-15 μm spectrum for 2MASS 0559 yielded the following parameters: T_{eff} = 1100 K, g = 316 m/s^2, K_{zz} = 4, C/O = 1.0, and [M/H] = 0. Table 5.3 highlights the best-fit model to 2MASS 0559, along with its associated χ^2 value, and compares this model with other models and their associated χ^2 values.

Figure 5.7 showcases that the best-fit PICASO model and its residual plot. Here we see that the depth of the CO absorption feature at 4.6 μm is accurately modeled, with the depth of the NH_3 absorption feature at 10.3 μm being slightly over-fit. There is also some slight under-fitting of the 1-2.5 μm peaks, particularly in the H- and K- bands. Unlike what was seen with 2MASS 0415, 2MASS 0559's best-fit model has less over- and under-fitting in the 3-5 μm region. We still struggle to fit the CO_2 feature.

In Figure 5.8, we showcase how varying the model temperature about the best-fit result for 2MASS 0559 by ±100 K. The choice of varying temperature by 100 K came about because above 1000 K, the steps in temperature for forward models is limited to just 100 K. Varying the temperature by 100 K has a significant impact on how well the mid-infrared region of 2MASS 0559 is modeled. When we decrease the temperature to 1000 K, we find that the model over-fits in the mid-infrared, and increasing the temperature to 1200 K under-fits the mid-infrared of 2MASS 0559. We also see in Table 5.3 that increasing and decreasing temperature yields worse χ^2 values than that of the best-fit model. This difference in χ^2 values compared to what was seen in 2MASS 0415 could be attributed to the fact that PICASO does not include variance of temperature by 50 K for models over 1000 K.

Table 5.3 This table summarizes how reduced χ^2 values of alternative models compare to the χ^2 value of 2MASS 0559's best-fit model. The best-fit model of 2MASS 0559's is highlighted in bold with double lines underneath. Each row afterwards showcases how χ^2 values differ when varying atmospheric parameters by one step. Each of the models presented in this table are plotted and compared to each other throughout this chapter.

Model	**Temperature (K)**	**log(K_{zz})**	**C/O**	**Reduced χ^2**
Best Fit	**1100**	**4**	**1.0**	**5.96**
Increase Temperature	1200	4	1.0	8.32
Decrease Temperature	1000	4	1.0	11.69
Increase log(K_{zz})	1100	7	1.0	9.51
Decrease log(K_{zz})	1100	4	1.0	7.03
Increase C/O	1100	4	1.5	7.10
Decrease C/O	1100	4	0.5	10.87

The next step in the analysis of 2MASS 0559 involves varying K_{zz} and C/O to see how these parameters affect model fits. In particular, we look to see how these parameters are able to fit CO, CO_2, and NH_3. Just as with 2MASS 0415, varying metallicity did not lead to significant changes in model fits; sub-solar and super-solar metallicities did not improve model fits.

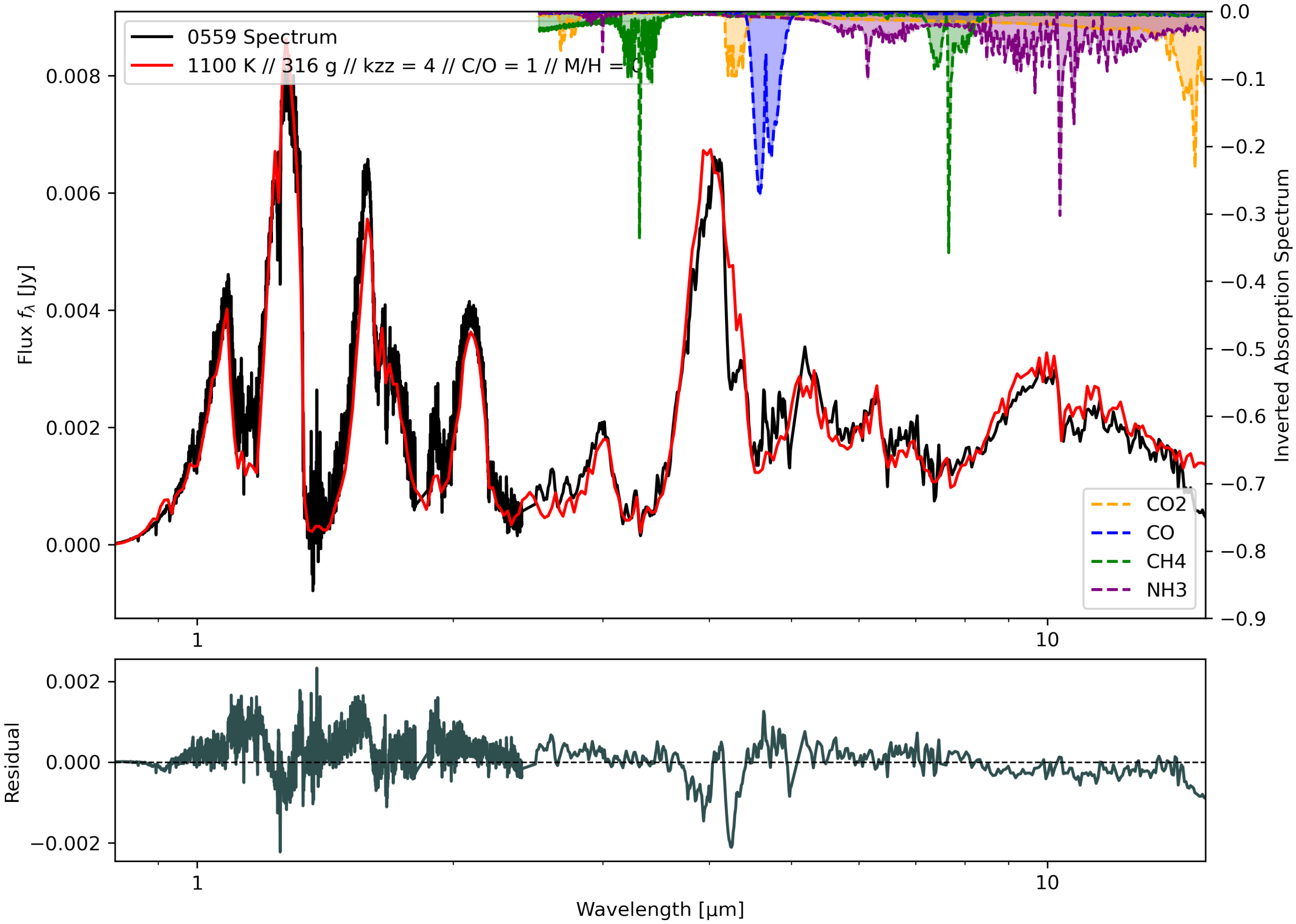

Figure 5.7 Plotted is the 1-15 µm spectrum for 2MASS 0559 (black) along with the best-fit PICASO disequilibrium model (red). Plotted invertedly on top is the absorption spectrum of CO_2 (orange), CO (blue), CH_4 (green), and NH_3 (purple). Here we see that the CO feature at 4.6 µm is accurately modeled, but the NH_3 feature at 10.3 µm is not as well fit. Plotted beneath the best-fit model is the residual between the best-fit model and the spectrum, which highlights regions where there is over- and under-fitting.

Figure 5.9 showcases how varying values of vertical mixing change models fits for models with temperature fixed at 1100 K. Increasing vertical mixing (K_{zz} of 7) yields significant change in how well the 3-5 µm is fit. In particular, we see over-fitting of the 4 µm peak and under-fitting of CO_2 and NH_3. Due to the significant over-fitting of the 4 µm peak, we find that increasing vertical mixing yields a high value of χ^2. With a higher value of K_{zz}, there is also some under-fitting in the near-infrared in the H- and K- bands, particularly with CH_4 in the H-band at 1.6 μm. While increasing vertical mixing does improve the fit to CO_2, it is at the cost of poorly fitting the rest of the spectrum. Decreasing vertical mixing (K_{zz} of 2) yields the worst fit to the CO_2 absorption feature, but there is better fit to the near-infrared region of 2MASS 0559.

Values of C/O were varied by steps of 0.5 to understand which parts of 2MASS 0559's spectrum are sensitive to variations of C/O. In Figure 5.10, we include model spectra with C/O values of 0.5, 1, and 1.5. Again, none of the C/O values are able to accurately capture the depth of the CO_2 absorption feature at 4.2 μm. Varying C/O does yield slight changes to the depth of the 4.6 μm CO absorption feature, but this change is not as significant as what was seen when changing values of K_{zz}. Additionally, decreasing C/O causes there to be an over-fitting of the 4 μm peak, which causes the associated χ^2 value to increase. On the other hand, increasing C/O causes there to be an under-fitting of the 4 μm peak. Varying C/O also has a small impact on the modeling of 1-2.5 μm region and the 5-15 μm region. Overall, the most variation in model fitting when changing values of C/O can be seen between 3-5 μm, with a big change in CH_4 at 1.6 μm.

Cushing et al. (2008)'s study of the atmospheric parameters of L- and T-dwarfs using ground-based observations and Spitzer included 2MASS 0559. They derived the following properties of 2MASS 0559: T_{eff} = 1200 K, g = 3162 m/s^2, and K_{zz} = 5. In their study K_{zz} was kept fixed, meaning that the extent of vertical mixing was held at a constant value. A year later, another study would follow up using ground-based and Spitzer observations allowing for the value of K_{zz} to vary (Stephens et al. 2009). The models used in their study were the predecessor of the Sonora family of models. They found the following best-fit parameters of 2MASS 0559: T_{eff} = 1200 K, g = 316 m/s^2, and K_{zz} = 2. While gravity values from PICASO are consistent with Stephens et al. (2009), temperatures and K_{zz} values slightly differ from those earlier studies. These differences could be attributed to the addition of AKARI data from 2.5-5 μm and from newer models that more effectively represent what is observed in substellar atmospheres.

In Mukherjee et al. (2024)'s study, see Figure 5.11, the best fit to the 2MASS 0559 2.5-15 µm spectrum had the following parameter values: T_{eff} = 1154 K, g = 46 m/s^2, K_{zz} = 1.07, C/O = 0.48, and [M/H] = 0.28. Table 5.4 compares the results of using PICASO to find best-fit parameters for the 1-15 µm to the results of Mukherjee et al. (2024). Between this work and theirs, there is close agreement in values of metallicity and temperature, while predicted values for gravity, vertical mixing, and C/O are not in agreement. Furthermore, in Figure 5.12, we showcase differences between best-fits for this study and that of Mukherjee et al. (2024). Mukherjee et al. (2024) obtains a slightly higher temperature than what we found, although we note an under-fitting of the 1-2.5 µm region when we plot their corresponding Elf-Owl model with 2MASS 0559's spectrum. This under-fitting is likely the result of Mukherjee et al. (2024)'s team not using ground observations for their study.

Table 5.4 The best-fit PICASO and Sonora Elf-Owls (Mukherjee et al. 2024) parameters to 2MASS 0559 across 1-15 µm and 2.5-15 µm, respectively.

Parameters from Best-Fit PICASO Disequilibrium Models for 2MASS 0559					
	Temperature (Kelvin)	Gravity (m/s^2)	Vertical Mixing (K_{zz})	C/O ratio	[M/H]
My PICASO best-fit	1100	316	4	1.0	0
Mukherjee et al. (2024)'s best-fit	1154	46	1.07	0.48	0.28

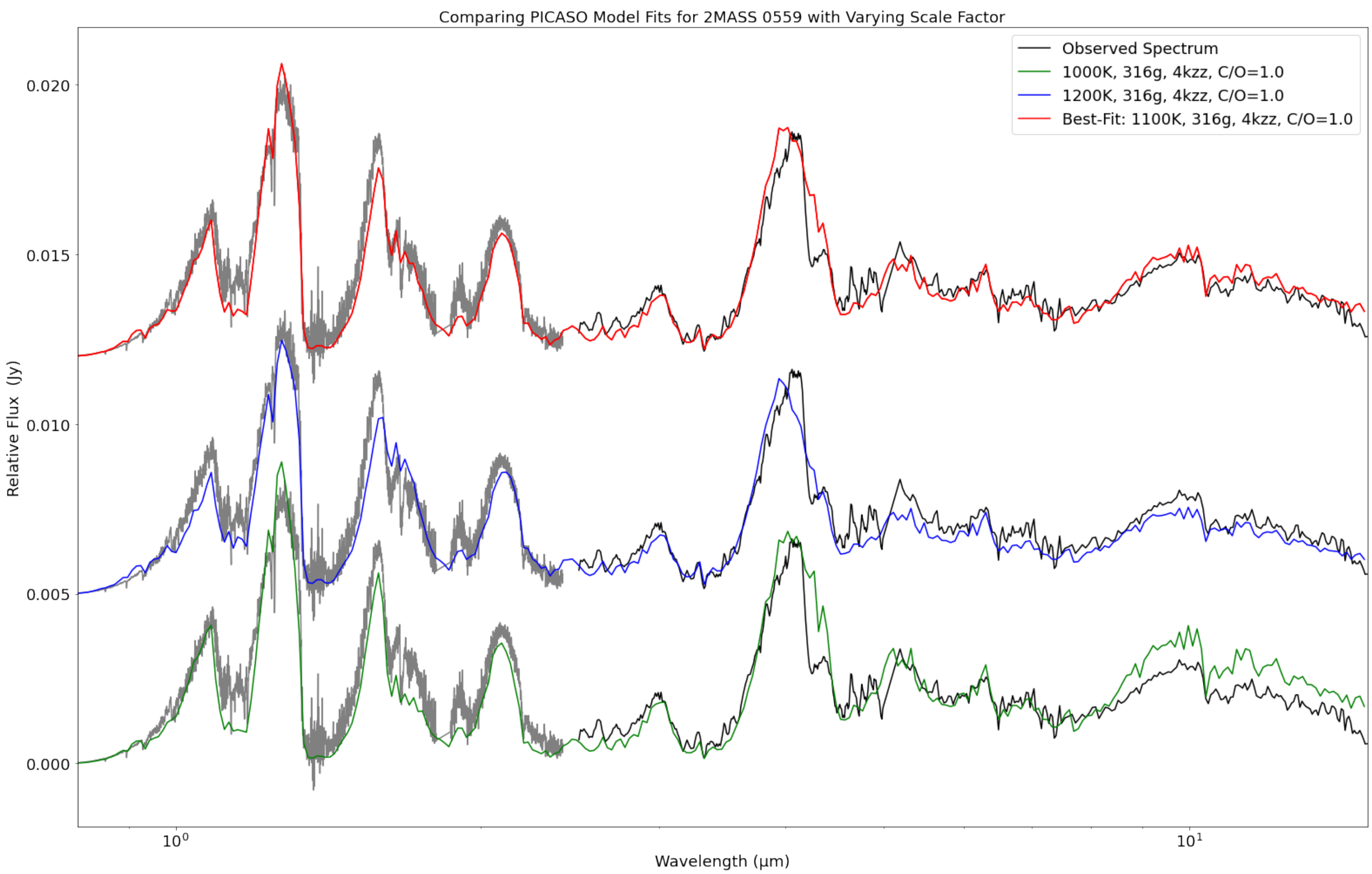

Figure 5.8 Plotted is the 1-15 μm spectrum for 2MASS 0559 (black) along with the best-fit PICASO disequilibrium model (red) and two models that share the same values for all parameters except for temperature. Each model is plotted with their corresponding scale factor. The model with temperature at 1000 K (green) has a poor fit to NH_3, while still maintaining a good fit to CO. The model with temperature at 1200 K (blue) over-fits NH_3, but does better in modeling CO_2.

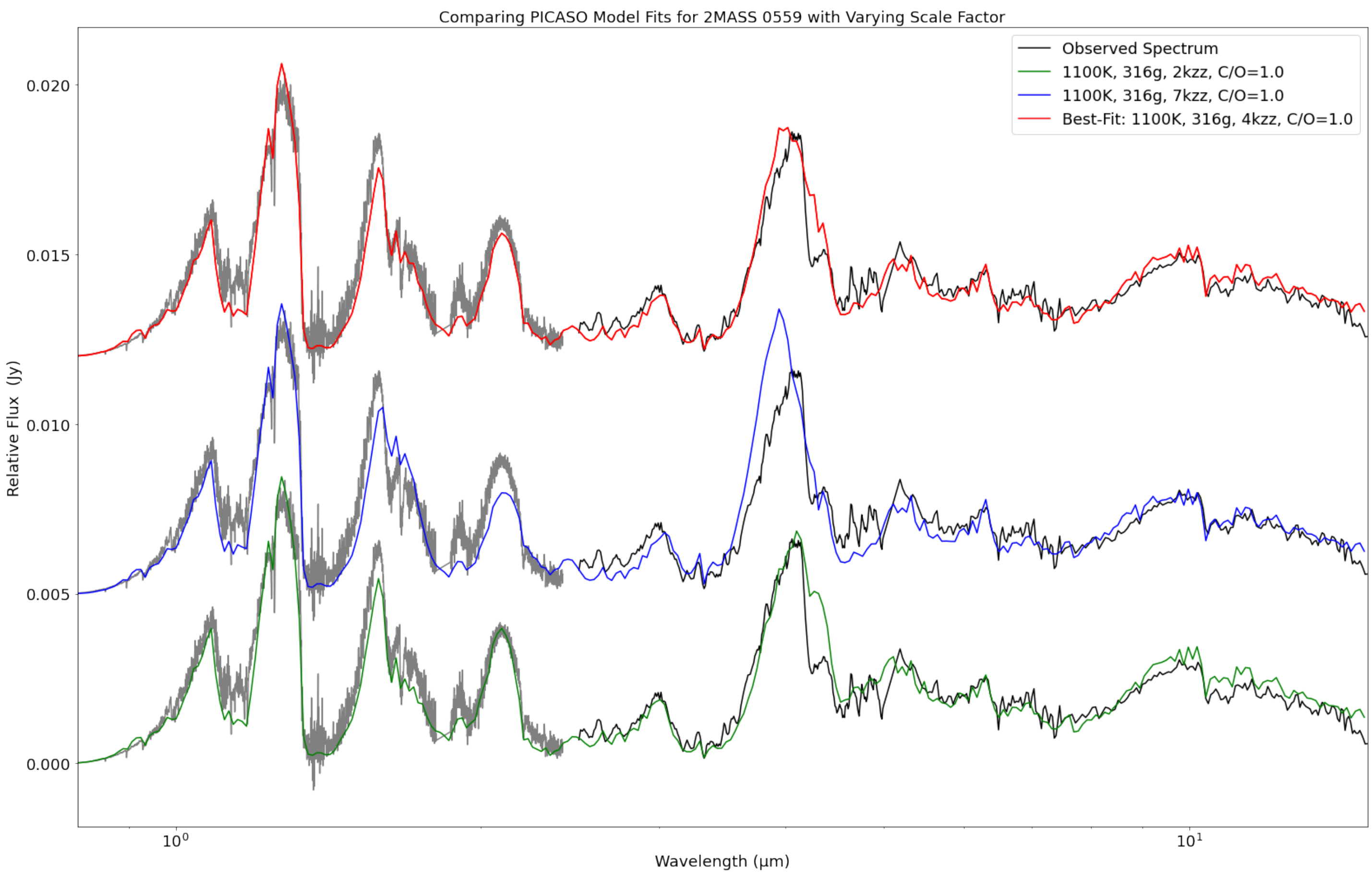

Figure 5.9 Plotted is the 1-15 µm spectrum for 2MASS 0559 (black) along with the best-fit PICASO disequilibrium model (red) and two models that share the same values for all parameters except for K_{zz}. Each model is plotted with their corresponding scale factor. Increasing K_{zz} (blue) from the best-fit leads to over-fitting of the 4 µm peak and CO, while maintaining a good fit to NH_3. Decreasing K_{zz} (green) leads to an under-fitting of the aforementioned molecules.

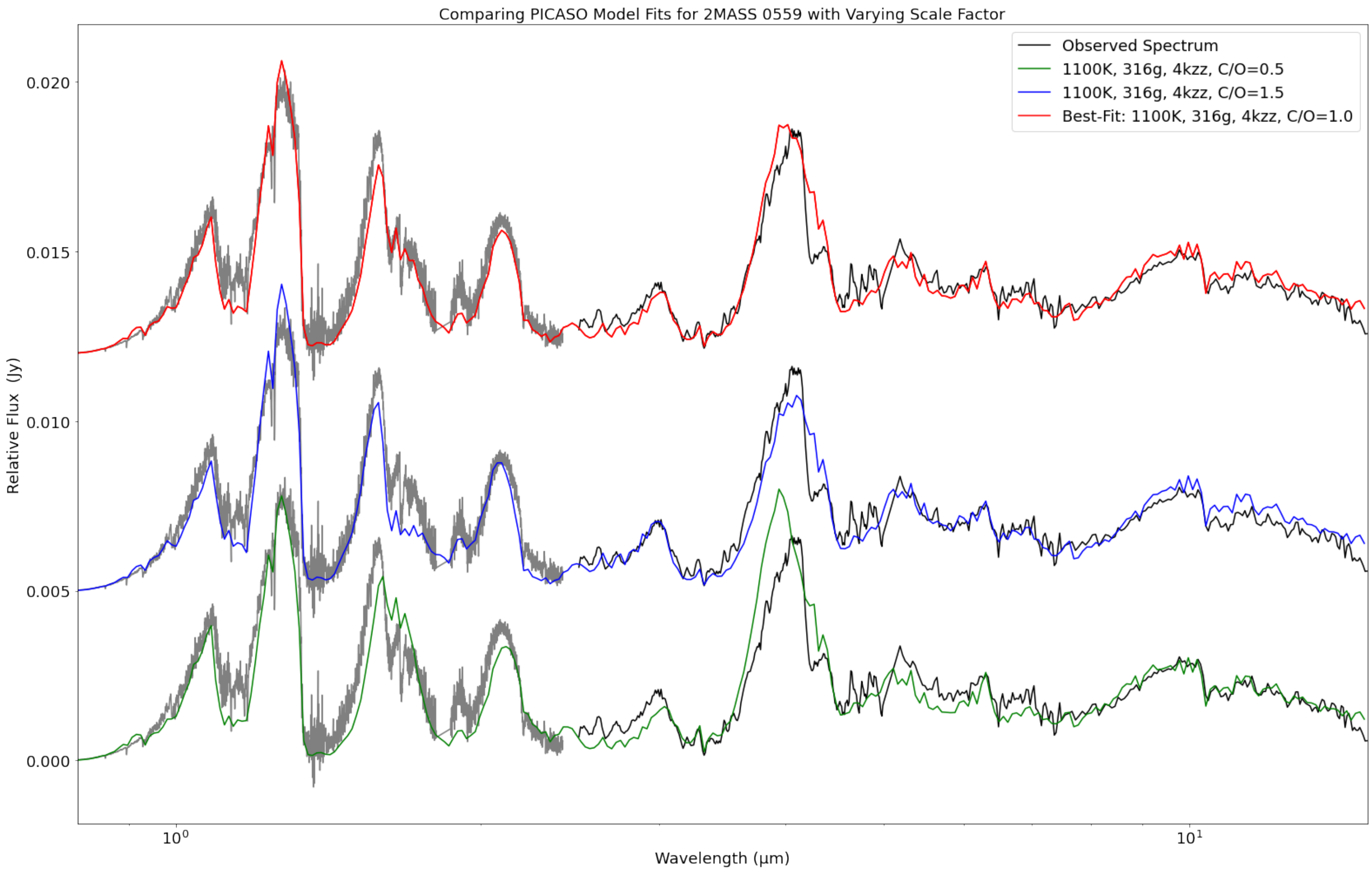

Figure 5.10 Plotted is the 1-15 μm spectrum for 2MASS 0559 (black) along with the best-fit PICASO disequilibrium model (red) and two models that share the same values for all parameters except for C/O. Each model is plotted with their corresponding scale factor. The higher value of for C/O at 1.5 (green) accurately models the NH_3 feature, while also providing a good fit to CO, but at the expense of overfitting 4 μm peak. While a C/O value of 0.5 (blue) still provides a good fit to CO, there is under-fitting of NH_3 and the 4 μm peak. We also see a significant change in how well CH_4 is modeled in the H-band at 1.6 μm. None of the models are able to accurately capture the depth of the CO_2 absorption feature.

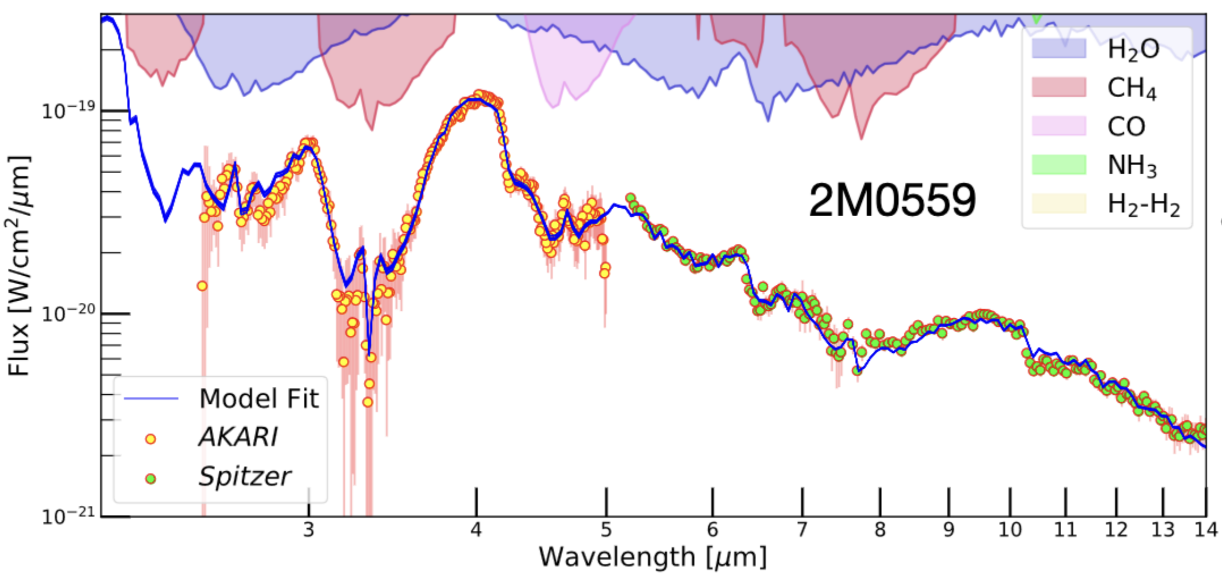

Figure 5.11 Best-fit Elf-Owl model to the 2.5-15 µm spectrum of 2MASS 0559 taken from Mukherjee et al. (2024). The spectrum from AKARI is represented by yellow circles and the spectrum from Spitzer is represented by green circles with the best-fit model in blue.

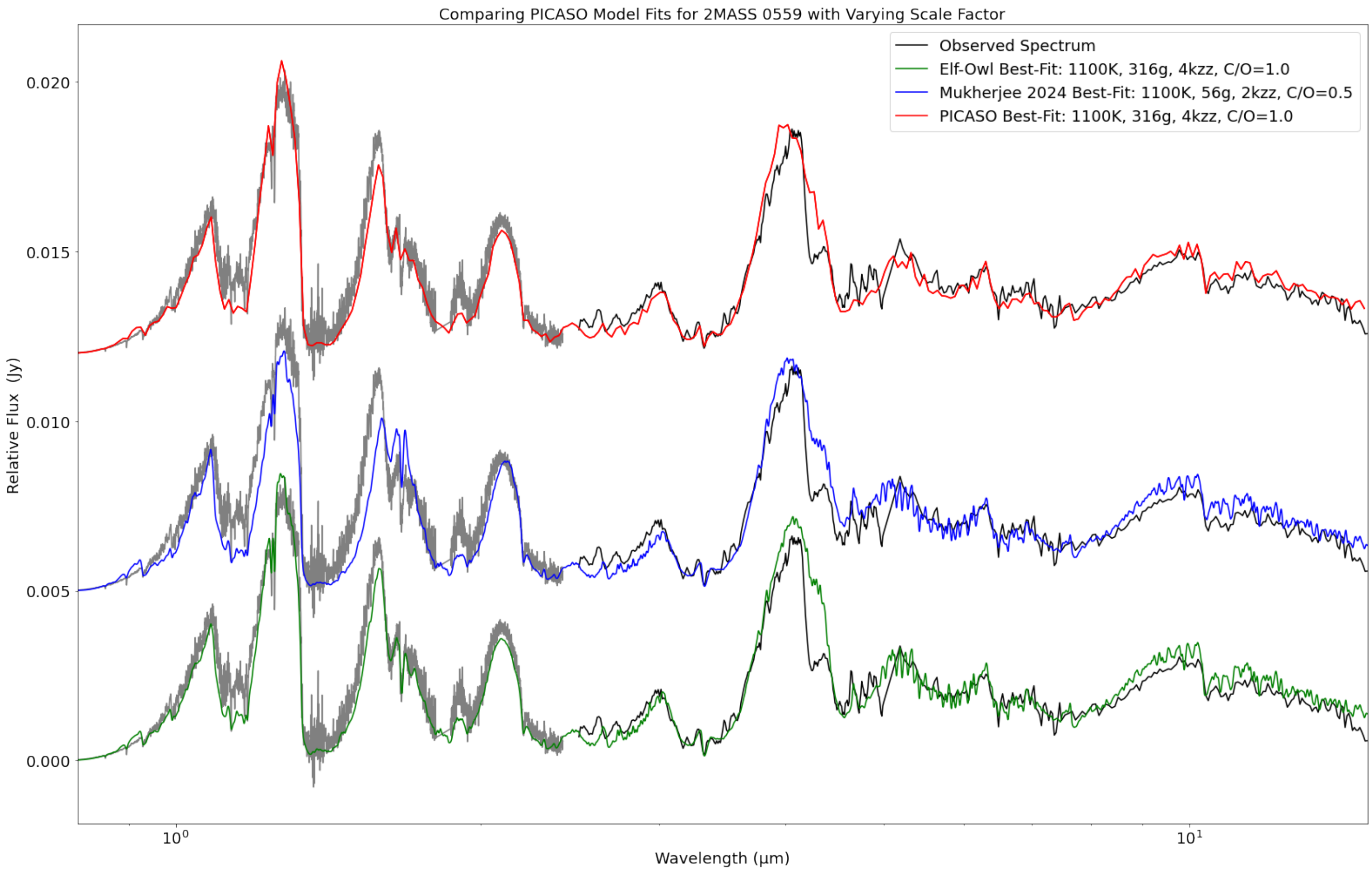

Figure 5.12 Best-fit PICASO (red) and Elf-Owl (green) models plotted with the best-fit model from Mukherjee et al. (2024) (blue). The model fits to the 2MASS 0559 spectrum across 3-15 μm is in general agreement, with major differences coming from the under-fitting of the 1-2.5 μm region from Mukherjee et al. (2024) . None of the models are able to accurately model the CO_2 feature. Discrepancies in the model fits can be attributed to the inclusion of 1-2.5 μm data in the analysis for this project. All models are plotted with their best-fit scale factor.

Chapter 6

Conclusions

Final remarks are presented along with how this project supports goals from the Astrophysics Research Program. In summary, the results of using PICASO to model the spectra of 2MASS 0415 and 2MASS 0559 have shown that metallicity has little effect on model fits, especially as it concerns modeling disequilibrium chemistry features. Vertical mixing and C/O, along with temperature, are parameters that play a significant role in creating accurate model fits to spectra. The best-fit PICASO models for the spectra of 2MASS 0415 and 2MASS 0559 struggle to accurately model the CO_2 absorption feature, which indicates that there is a need to improve understanding on what drives the abundance of CO_2 that is observed. Future avenues using the results of this project are discussed at the end of this chapter.

6.1 Summary

Using the binary fitting code (Turner et al. 2025) to find best-fit parameters using Sonora foward models, PICASO disequilibrium chemistry models were created to model the 1-15 µm spectra of 2MASS 0415 and 2MASS 0559. PICASO's inclusion of molecular chemistry allows us to explore how parameters, such as K_{zz} and C/O can explain the molecular features in these two T-dwarfs.

Due to the small sample size, no statistical conclusions on the best-fit parameters of T-dwarfs can be made. More work is needed on a larger sample of T-dwarfs to be able to make any statistical conclusions.

Although no statistical conclusions can be made, final comments on the characteristics of 2MASS 0415 and 2MASS 0559 can be presented. Both T-dwarfs have low values of eddy diffusion, meaning that the extent of vertical mixing is low in the atmospheres of 2MASS 0415 and 2MASS 0559. The effects of metallicity on modeling the spectra of 2MASS 0415 and 2MASS 0559 are not as notable as eddy diffusion and C/O. C/O can be used to account for the abundance of CO, but struggles to accurately model the CO_2 absorption feature seen in the mid-infrared of the spectra of these two T-dwarfs. As such, there is a need for increased observations of T-dwarfs in the mid-infrared, as well as more laboratory experimentation to better constrain the presence of CO_2 in cool atmospheres. Further studies of mid to late T-dwarfs of greater sample size than this thesis that cover the spectral range of 1-15 µm are needed so that they may shed more light on this.

The study of the atmospheres of brown dwarfs supports a number of goals of the Astrophysics Research Program. Firstly, this study furthers the program's goal of exploring the evolution of stars and planets. In particular, this work has furthered the understanding of how vertical mixing and C/O contribute to molecules observed in the upper atmospheres of T-dwarfs. Secondly, this work supports the program's goal of discovering the secrets of the Universe. This study has explored how temperature, vertical mixing, C/O, and metallicity affect the spectra of two T-dwarfs and sheds light on how these parameters affect the spectrum of cool dwarfs. Thirdly, the results of this project support the program's goal of exploring the possibility of life on exoplanets. Although brown dwarfs are not believed to have the potential to host life, cooler dwarfs are considered to be analogs to exoplanets due to their cool temperatures, small sizes, and complex atmospheric and molecular structure. Furthermore, the modeling techniques that are used to study cooler dwarfs can also be used on exoplanets. These modeling techniques, including PICASO, are refined as studies of cooler dwarfs push the boundaries of the understanding of cool atmospheres.

6.2 Future Work

Using the Jupyter Notebooks that were created to model the atmospheres of 2MASS 0415 and 2MASS 0559, there are many avenues of exploration that can be taken in future projects. One possible avenue is creating binary fits to 2MASS 0559 using PICASO.

Additionally, future students will be able to analyze spectra of brown dwarfs with more ease using the Jupyter Notebooks that have been created to use PICASO to make disequilibrium fits. Particularly, members of our research group are currently working to reduce JWST spectra in preparation of analyzing the spectra using PICASO. Furthermore, a member of our group has stitched together some of the other AKARI spectra to ground-based and Spitzer observations of L- and T-dwarfs, which can now be analyzed with more ease using PICASO.

Future work is needed to further explore the patterns of best-fit parameters that are seen in the spectra of cool dwarfs and how these are similar and different from that of results from other research groups. To make any conclusions on the nature of T-dwarfs, more observations are needed, as well as further probing of the 2.5-5 μm spectral range. Currently, this can only be done using data from AKARI or JWST. Beiler et al. (2024a) has already seen variations in the spectra of T-dwarfs and this project further showcases some of the peculiarities seen in the flux and absorption features in the spectra of cool T-dwarfs.

The study of brown dwarf atmospheres is still growing as we continue to conduct observations and improve on models. With future observations using JWST and other surveys, we can further our understanding of cooler atmospheres, especially that of exoplanets—and the Universe as a whole.

Bibliography

Beiler, S. A., Cushing, M. C., Kirkpatrick, J. D., Schneider, A. C., Mukherjee, S., Marley, M. S., Marocco, F., & Smart, R. L. 2024a, Precise Bolometric Luminosities and Effective Temperatures of 23 late-T and Y dwarfs Obtained with JWST

Beiler, S. A., Mukherjee, S., Cushing, M. C., Kirkpatrick, J. D., Schneider, A. C., Kothari, H., Marley, M. S., & Visscher, C. 2024b, A Tale of Two Molecules: The Underprediction of CO_2 and Overprediction of PH_3 in Late T and Y Dwarf Atmospheric Models

Brock, L. S., Barman, T., Konopacky, Q. M., & Stone, J. M. 2021, Cloud Properties of Brown Dwarf Binaries Across the L/T Transition

Burgasser, A., Burrows, A., & Kirkpatrick, J. D. 2006a, The Astrophysical Journal, 639, 1095–1113

Burgasser, A., Kirkpatrick, J., & Brown, M. 2001, 169

Burgasser, A. J., Geballe, T. R., Leggett, S. K., Kirkpatrick, J. D., & Golimowski, D. A. 2006b, ApJ, 637, 1067

Burningham, B., et al. 2021, Monthly Notices of the Royal Astronomical Society, 506, 1944–1961

Burrows, A., Hubbard, W. B., Lunine, J. I., & Liebert, J. 2001, Reviews of Modern Physics, 73, 719–765

Cushing et al. 2008, The Astrophysical Journal, 678, 1372–1395

Cushing, M. C., Rayner, J. T., & Vacca, W. D. 2005, The Astrophysical Journal, 623, 1115–1140

Cushing, M. C., et al. 2006, The Astrophysical Journal, 648, 614

Dupuy, T. J., & Liu, M. C. 2012, The Astrophysical Journal Supplement Series, 201, 19

Hauschildt, P., Wehrse, R., Starrfield, S., & Shaviv, G. 1992, Astrophysical Journal, 393, 307

Hauschildt, P. H., Allard, F., Alexander, D. R., & Baron, E. 1997, ApJ, 488, 428

Hauschildt, P. H., Allard, F., Ferguson, J., Baron, E., & Alexander, D. R. 1999, ApJ, 525, 871

Karalidi, T., Marley, M., Fortney, J. J., Morley, C., Saumon, D., Lupu, R., Visscher, C., & Freedman, R. 2021, The Astrophysical Journal, 923, 269

Kirkpatrick, J. D. 2005, ARA&A, 43, 195

Kirkpatrick, J. D., et al. 1999, The Astrophysical Journal, 519, 802

Knapp, G. R., et al. 2004, The Astronomical Journal, 127, 3553–3578

Kumar, S. S. 1963, Astrophysical Journal, 137, 1121

Lodders, K., & Fegley, B. 2002, Icarus, 155, 393

Looper, D. L., et al. 2008, The Astrophysical Journal, 686, 528

Marley, M., & Robinson, T. 2015, Annual Review of Astronomy and Astrophysics, 53, 279–323

Marley, M., Saumon, D., Morley, C., Fortney, J., Visscher, C., Freedman, R., & Lupu, R. 2021

McLean, I. S., McGovern, M. R., Burgasser, A. J., Kirkpatrick, J. D., Prato, L., & Kim, S. S. 2003, ApJ, 596, 561

Morley, C. V., et al. 2024, The Sonora Substellar Atmosphere Models. III. Diamondback: Atmospheric Properties, Spectra, and Evolution for Warm Cloudy Substellar Objects

Mukherjee, S., Batalha, N. E., Fortney, J. J., & Marley, M. S. 2023, The Astrophysical Journal, 942, 71

Mukherjee, S., Fortney, J. J., Batalha, N. E., Karalidi, T., Marley, M. S., Visscher, C., Miles, B. E., & Skemer, A. J. I. 2022, The Astrophysical Journal, 938, 107

Mukherjee, S., et al. 2024, arXiv e-prints, arXiv:2402.00756

Murakami, H., et al. 2007, Publications of the Astronomical Society of Japan, 59, S369–S376

Nakajima, T., Oppenheimer Osorio, B. R., Kulkarni, S. R., Golimowski, D. A., Matthews, K., & Durrance, S. 1995, Nature, 378, 463

Noll, K. S., Geballe, T. R., & Marley, M. S. 1997, The Astrophysical Journal, 489, L87

Onaka, T., et al. 2007, Publications of the Astronomical Society of Japan, 59, S401–S410

Rebolo, R., Martín, E. L., Basri, G., Marcy, G. W., & Zapatero-Osorio, M. R. 1996, The Astrophysical Journal, 469, L53–L56

Robello, R., Zapatero Osorio, M. R., & Martín, E. L. 1995, Nature, 377, 129

Saumon, D., Geballe, T. R., Leggett, S. K., Marley, M. S., Freedman, R. S., Lodders, K., Fegley, Jr., B., & Sengupta, S. K. 2000, The Astrophysical Journal, 541, 374–389

Saumon, D., & Marley, M. S. 2008, The Astrophysical Journal, 689, 1327–1344

Sorahana, S., & Yamamura, I. 2012, The Astrophysical Journal, 760, 151

Stephens, D. C., et al. 2009, The Astrophysical Journal, 702, 154–170

Tarter, J. 1985, Astrophysics of Brown Dwarfs; Proceedings of the Workshop

Tokunaga, A. T., Simons, D., & Vacca, W. D. 2002, Publications of the Astronomical Society of the Pacific, 114, 180–186

Turner, S. K., Stephens, D. C., Scoresby, C. B., & Miller, J. A. 2025, A Survey Of Model Fits to Brown Dwarf Spectra Through the L-T Sequence

Visscher, C., & Moses, J. I. 2011, The Astrophysical Journal, 738, 72

Werner, M. W., et al. 2004, The Astrophysical Journal Supplement Series, 154, 1–9

Yamamura, I., Tsuji, T., & Tanabé, T. 2010, The Astrophysical Journal, 722, 682–698